A Synaptotagmin isoform switch during the development of an identified CNS synapse

Olexiy Kochubey[1], Norbert Babai[1, 2], Ralf Schneggenburger[1]

[1] Laboratory of Synaptic Mechanisms, Brain-Mind Institute, École Polytechnique Fédérale de Lausanne, 1015 Lausanne, Switzerland

[2] present address: Institute of Animal Physiology & Department of Biology, Universität Erlangen-Nürnberg, 91058 Erlangen, Germany

Correspondence:

Ralf Schneggenburger (ralf.schneggenburger@epfl.ch) or

Olexiy Kochubey (olexiy.kochubey@epfl.ch)

Laboratory of Synaptic Mechanisms

Brain Mind Institute

École Polytechnique Fédérale de Lausanne (EPFL)

CH-1015 Lausanne

Switzerland

Char count: 71208 chars

Various Synaptotagmin (Syt) isoform genes are found in mammals, but it is unknown whether Syts can function redundantly in a given nerve terminal, or whether isoforms can be switched during the development of a nerve terminal. Here, we investigated the possibility of a developmental Syt isoform switch using the calyx of Held as a model synapse. At mature calyx synapses, fast Ca^{2+} - driven transmitter release depended entirely on Syt2, but the release phenotype of Syt2 knock-out (KO) mice was weaker at immature calyces, and absent at pre-calyceal synapses early postnatally. Instead, conditional genetic inactivation shows that Syt1 mediates fast release at pre-calyceal synapses, as well as a fast release component resistant to Syt2 deletion in immature calyces. This demonstrates a developmental Syt1 - Syt2 isoform switch at an identified synapse, a mechanism that could fine-tune the speed, reliability and plasticity of transmitter release at fast releasing CNS synapses.

Introduction

Fast information transfer between neurons is mediated by the process of chemical synaptic transmission. Nerve terminals contain a highly specialized vesicle fusion machinery consisting of SNAREs and associated proteins, to translate the action-potential (AP) driven rise of presynaptic Ca^{2+} into a precise and fast phase of transmitter release (Goda and Stevens, 1994; Sabatini and Regehr, 1996; Südhof, 2013; Schneggenburger and Rosenmund, 2015). Synaptotagmins (Syts), a family of Ca^{2+} binding proteins with double C2 domains, are central to the triggering of fast transmitter release by Ca^{2+}. Gene deletion studies have shown that inactivation of the Syt1 gene abolishes fast release in mice and in drosophila synapses (Littleton et al., 1993; Geppert et al., 1994; Yoshihara and Littleton, 2002; Nishiki and Augustine, 2004). Multiple lines of evidence show that Syts are Ca^{2+} sensors for fast vesicle fusion. Thus, a highly nonlinear Ca^{2+} sensing mechanism found in neurons and secretory cells (Thomas et al., 1993; Heidelberger et al., 1994; Heinemann et al., 1994; Bollmann et al.,

2000; Schneggenburger and Neher, 2000) is abolished upon genetic deletion of Syt1, or modified when point mutations are introduced at critical sites (Fernández-Chacón et al., 2001; Yoshihara and Littleton, 2002; Sorensen et al., 2003; Sun et al., 2007; Kochubey and Schneggenburger, 2011).

Interestingly, a large number of Syt genes is present in the genome of mammals (~ 17; Craxton, 2010); of these, Syt1, 2, 3, 5, 6, 7, 9 and 10 bind Ca^{2+} (Pang and Südhof, 2010). Syts are differentially expressed between tissues, and can therefore mediate physiologically different forms of release across secretory systems. For example, Syt1 and Syt7 are Ca^{2+} sensors for catecholamine release in chromaffin cells (Voets et al., 2001; Schonn et al., 2008), and Syt10 was shown to mediate IGF-1 release from the somatodendritic compartment of olfactory neurons (Cao et al., 2011). For fast transmitter release at brain synapses, Syt2, an isoform gene present in many vertebrates (Craxton, 2010), has to be considered in addition to Syt1. Syt2 has a high sequence homology to Syt1, and is, in general, expressed in hindbrain areas (Geppert et al., 1991; Berton et al., 1997; Pang et al., 2006a). Consistent with the expression data, genetic deletion of Syt2 suppresses fast release at the calyx of Held and at the neuromuscular junction (Pang et al., 2006a; Sun et al., 2007; Kochubey and Schneggenburger, 2011; Wen et al. 2010). In rescue experiments in cultured forebrain neurons, only Syt1, -2 and -9 were able to recover the release phenotype of Syt1 KO mice, a finding which identified Syt9 as a putative Ca^{2+} sensor for release besides Syt1 and Syt2 (Xu et al., 2007). Since several Syt proteins can act as fast Ca^{2+} sensors, it is possible that Syts function redundantly in synaptic transmission, or that Syts are exchanged against each other during the development of a given nerve terminal. However, these possibilities have so far received little attention (but see Cooper and Gillespie, 2011).

During brain development, synaptic connections are structurally and functionally adapted to fulfil the specific computational needs of the circuits in which they are embedded. A good example is the highly specialized calyx of Held synapse in the auditory brainstem, a synapse formed between a subtype of bushy cells of the ventral cochlear nucleus (VCN), and a principal neuron of the medial nucleus of the trapezoid body (MNTB) (Borst and Soria van Hoeve, 2012). The formation of the calyx synapse essentially proceeds in three steps. First, small excitatory synapses are established onto MNTB neurons at around birth; we will refer to these synapses as "pre-calyceal synapses" (Fig. 1A; Hoffpauir et al., 2010). Second, at postnatal days 2 - 3 (P2 - P3), pre-calyceal synapses grow in an abrupt process, and competing synapses are eliminated (Hoffpauir et al., 2006; Rodriguez-Contreras et al., 2008; Xiao et al., 2013). Third, following the establishment of the one-to-one connectivity, further refinement in the structure and function of the calyx synapse occur, which together with the large terminal size optimizes fast AP-mediated transmitter release and rapid postsynaptic depolarization (Iwasaki and Takahashi, 1998; Taschenberger et al., 2002; Fedchyshyn and Wang, 2005; see Borst and Soria van Hoeve 2002, for review and further references). However, the possibility of developmental isoform switches of major presynaptic proteins involved in release control have so far received little attention. The calyx synapse, which can be unambiguously identified in physiological recordings throughout postnatal development, should be an ideal model system to study expression changes of presynaptic proteins and their functional consequences.

Here, we demonstrate a Syt isoform switch at an identified synapse, the calyx of Held. We found that fast transmitter release at pre-calyceal synapses was *independent* of Syt2 removal, and that in the following one to two weeks of development, the release phenotype of Syt2 KO mice develops gradually. This developmental dependence called for an additional Ca^{2+} sensor expressed early postnatally. Using a novel floxed allele of Syt1, we show that a majority of

fast release of pre-calyceal synapses depends on Syt1. Similarly, a fast release component in immature calyces of Syt2 KO mice was significantly reduced upon additional genetic inactivation of Syt1. On the other hand, Syt9 did not have a detectable contribution to Ca^{2+} -evoked release early postnatally. Thus, our study demonstrates a functional Syt1 to Syt2 isoform switch during the development of an identified CNS synapse.

Results

Fast release from pre-calyceal synapses does not depend on Syt2

Syt2 is a Synaptotagmin isoform widely expressed in caudal brain regions such as brainstem, cerebellum, spinal cord and neuromuscular junction (Geppert et al., 1991; Marqueze et al., 1995; Berton et al., 1997; Fox and Sanes, 2007), and Syt2 KO mice perish after 2 - 3 weeks of age (Pang et al., 2006a). However, newborn Syt2 KO mice are indistinguishable from their littermate controls, and the motor deficits and the body weight loss in Syt2 KO mice develop progressively during the first two postnatal weeks (Pang et al., 2006a). Therefore, it is possible that synapses in the caudal brain regions become critically dependent on Syt2 only during postnatal development. Given that the calyx of Held projection is located in the hindbrain and utilizes Syt2 as its major presynaptic Ca^{2+} sensor at ~ two weeks of age, we hypothesized that early in development, transmitter release at this synapse might be less dependent on Syt2.

To verify this hypothesis, we used a conventional Syt2 KO mouse (Pang et al., 2006a) and investigated its release phenotype at different developmental stages of the calyx synapse (see Fig. 1A for a scheme; see Introduction for references). We first recorded fiber-stimulation evoked EPSCs in MNTB neurons of Syt2 KO mice and their littermate control mice at postnatal days (P) 2 - 3. Surprisingly, we found EPSCs with similar peak amplitudes and risetimes in Syt2 KO mice ($Syt2^{-/-}$), and in littermate control mice ($Syt2^{+/+}$; Fig. 1B, C, D).

The frequency and amplitude of spontaneous EPSCs, which can be regarded as miniature EPSCs (mEPSCs), were also unchanged (Fig. 1B, C, E).

We next investigated whether postnatal development of the calyx of Held synapse would gradually reveal the Syt2 KO phenotype. At P5 - P6, we observed large EPSCs which depended in an all-or-none fashion on stimulus intensity (not shown), showing that these EPSCs arise from single calyx of Held inputs. At this age, the EPSC rise times were significantly faster than at P2-P3, consistent with a developmental speeding of transmitter release (Taschenberger et al., 2002; Fedchyshyn and Wang, 2005; Leão and von Gersdorff, 2009). At P5-P6, the EPSC amplitude was significantly reduced in Syt2 KO mice as compared to control (~ 4 - fold; Fig. 1F, G, H; $p < 0.05$). Furthermore, the EPSC risetimes were ~ 2 - fold slowed in Syt2 KO synapses (Fig. 1H; $p < 0.001$). The frequency of spontaneous events was ~ 7 fold higher in Syt2 KO mice than in control mice, but the mEPSC amplitude was unchanged (Fig. 1F, G, I). Thus, in contrast to P2 - P3 synapses, Syt2 is required at P5-P6 to support fast synchronous release and to clamp spontaneous release. However, there is still a significant amount of phasic, AP-evoked release that remains (~ 20%; Fig. 1G, H).

We hypothesize that AP-driven release at P2-P3 does not show a requirement for Syt2 because this isoform is not expressed at this stage of development. To test this, we performed immunohistochemistry with an anti-Syt2 antibody, using VGlut2 as a marker for glutamatergic terminals (Fig. 1J). At P0, we observed small VGluT2-positive puncta but no large calyx-type synapses, indicating the presence of only small pre-calyceal synapses at this age (Hoffpauir et al., 2006; Rodriguez-Contreras et al., 2008; Xiao et al., 2013). These terminals were virtually devoid of Syt2 (Fig. 1J, top). At this age, we noticed VGluT2 puncta expressing Syt2 only at the medial extremity of the MNTB (Fig. S1). At P2, there was still

little or no Syt2 signal in VGluT2 - positive nerve terminals. In contrast, at P5, elongated VGluT2-positive presynaptic structures representing immature calyces were present, and these terminals clearly expressed Syt2 (Fig. 1J, bottom). These data suggest a delayed expression onset of Syt2, at around the time when pre-calyceal synapses change their form and grow into large terminals.

Intrinsically fast release disappears during development of Syt2 KO mice

The results of Fig. 1 suggest that the Syt2 KO phenotype at the calyx of Held synapses develops progressively with postnatal maturation. To study this possibility in more detail, we next studied the development of the KO phenotype in presynaptic Ca^{2+} uncaging experiments. With uncaging, a spatially homogenous Ca^{2+} signal is created, which allows us to directly study the role of Syt2 the intrinsic release kinetics (Wölfel et al., 2007). We studied transmitter release in Syt2 KO synapses, comparing three postnatal age groups: P5 - P6 (the earliest age amenable to paired recordings; immature calyces), P8 - P10 (an intermediate age) and P13 - P15 (mature calyces) (Fig. 2A-C). Presynaptic Ca^{2+} uncaging triggered fast EPSCs at P5 - P6 synapses (Fig. 2A1), smaller and slightly more slowly rising EPSCs at P8 - P10 (Fig. 2B1), and only slow release at P13 - P15 (Fig. 2C1). This directly demonstrates that intrinsically fast transmitter release gradually disappears with development of Syt2 KO calyces, as opposed to a possible deficit in Ca^{2+} channel - vesicle coupling which has also been observed in Syt2 mutants (Young and Neher, 2009).

We next analyzed the developmental disappearance of fast release in Syt2 KO mice by EPSC deconvolution to derive release rates (Fig. 2A2-C2; Neher and Sakaba, 2001). In response to flashes which elevated $[Ca^{2+}]_i$ to 10 - 30 µM, peak release rates were about 100 ves /ms in immature calyx synapses (P5 - P6), dropped to ~ 30 ves/ms at P8 - P10, and were well below 10 ves/ms in mature calyces at P13 - P15 (Fig. 2A2-C2; Fig. 2D). The integrated release rate

traces could be fitted with double exponential functions at P5-P6, with a fast release component with time constant ~ 3 ms accounting for ~ 500 vesicles in these Syt2 KO synapses (Fig. 2A2; Fig. 2E, F, grey bars). Note that this fast release component is somewhat slower, and clearly smaller than fast release observed in Syt2 wild-type calyces (not shown). Nevertheless, vigorous fast release is present in Syt2 KO calyces at P5-P6, which then becomes slower and smaller, and finally disappears at ~ P13 (Fig. 2A2 - C2; Fig. 2D-F). At P13 - P15, the cumulative release rate traces show a slow, sigmoidal rise (Fig. 2C2), indicating excessively slow release time constants of ~ 280 ms (Fig. 2C2; Fig. 2E, open red bar). In parallel to the development of the fast release phenotype, the frequency of spontaneous release increased with development in Syt2 KO synapses (Fig. 2 A3 - C3; Fig. 2G). Together with the data in Fig. 1, this demonstrates that the Syt2 KO phenotype at the calyx of Held develops gradually. We hypothesize, therefore, that early-on a fast Ca^{2+} sensor different from Syt2 must be present, which is then gradually downregulated with postnatal development.

To investigate how the remaining Ca^{2+} sensor influences the Ca^{2+} sensitivity of release in Syt2 KO calyces, we next constructed dose-response curves of peak transmitter release in Syt2 KO calyces at two age groups (P5 - P6 and P13 - P15; Fig. 2H, I). This is relevant because release remaining in Syt2 KO mice has been assigned to the action of a slow sensor (Sun et al., 2007). At P13 - P15, we found shallow dose-response curves, which could be fitted with a line with slope of 0.85 in double-logarithmic coordinates (Fig. 2H, grey data points). At P5 - P6, however, peak release rates were significantly higher, and a slope of 1.57 was found (Fig. 2H). Thus, differences in the estimates of the Ca^{2+} cooperativity of the remaining slow Ca^{2+} sensor, which were ~ 2 in the original study (Sun et al., 2007) but only ~ 1 in subsequent studies (Kochubey and Schneggenburger, 2011; Babai et al., 2014), are probably caused by differences in the age of the investigated Syt2 KO mice.

We further wished to study whether a loss of vesicle docking had contributed to the complete loss of the fast release component in Syt2 KO mice at P13 - P15. A previous study has reported a function of Syt1 in vesicle docking in chromaffin cells (de Wit et al., 2009). We reconstructed entire active zones of calyx synapses using transmission electron microscopy, and found no significant differences in the number of docked vesicles, in vesicle densities, nor in active zone size between Syt2 KO and control (Fig. S2). This shows that Syt2 primarily functions as a Ca^{2+} sensor for vesicle fusion but that Syt2 is not involved in vesicle docking, similar to the conclusionreached recently for Syt1 in hippocampal synapses (Imig et al., 2014).

Syt9 is not a Ca^{2+} sensor at immature calyx synapses

We next wished to identify which Ca^{2+} sensor is used by the calyx of Held synapse of young mice. A previous single-cell qPCR study found that Syt9 is expressed in bushy cells of young rats (Xiao et al., 2010; Syt9 was referred to as Syt5 therein). Since Syt9 can, in principle, mediate fast release besides Syt1 and Syt2 (Xu et al., 2007), we next wished to study the role of Syt9 early postnatally.

We first verified the developmental expression pattern of Syt1, Syt2 and Syt9 in the cochlear nucleus by qPCR (Fig. 3A). We found that Syt9 was expressed early in development (P1, P3 and P6) and was down-regulated thereafter, whereas Syt2 was initially weakly expressed, and then upregulated with postnatal development. Syt1 expression was stable; note, however, that expression on the mRNA level in the entire VCN is not necessarily equal to protein expression at specific output synapses. Nevertheless, the qPCR findings, together with immunohistochemical evidence (Fig. S3) and the previous single-cell qPCR results (Xiao et

al., 2010) suggest that Syt9 is initially expressed at detectable levels, and is then developmentally downregulated.

To test the role of Syt9 as a Ca^{2+} sensor at immature calyx synapses, we used a Syt9 KO mouse (Xu et al., 2007; see Experimental Procedures). Syt9 protein levels as tested by Western blot analysis in several brain regions were strongly reduced in Syt9 KO samples (Fig. 3B). We next recorded fiber-stimulation evoked EPSCs in Syt9 KO mice and their control littermate mice at P1 - P2, to test the function of Syt9 at a developmental stage at which release was independent of Syt2 (Fig. 1). Evoked EPSCs had similar amplitudes and rise times in Syt9 KO mice and in Syt9 control mice (Fig. 3C - E). Interestingly, the mEPSC frequency had a tendency to be larger in Syt9 KO synapses (n = 26 recordings) as compared to wild-type synapses (n = 23); but the statistical significance of this difference was only suggestive ($p = 0.051$; Fig. 3F). Thus, Syt9 was clearly not necessary for evoked release, and had only a subtle effect on release clamping at pre-calyceal synapses at P1-P2.

We next investigated whether the fast release component resistant to Syt2 KO in immature calyces at P5- P6 (Fig. 2), could be mediated by Syt9. For this purpose, we generated Syt2 - Syt9 DKO mice by crossing the two lines. Syt2 - Syt9 DKO mice were viable until at least P16, similar to the survival of Syt2 KO mice. We then made simultaneous pre- and postsynaptic recordings at the calyx synapse of young mice (P6 - P8), and evoked transmitter release by pool-depleting presynaptic depolarizations of 50 ms. As expected from the Ca^{2+} uncaging data (Fig. 2), calyces in juvenile Syt2 KO mice showed a prominent fast release component resistant to the deletion of Syt2 (data traces not shown). However, this fast release component was also observed in Syt2 - Syt9 DKO mice (Fig. 3G). Neither the EPSC amplitudes nor their risetimes were changed significantly (Fig. 3H). Similarly, the parameters of fast and slow release as analyzed by EPSC deconvolution were unchanged in Syt2 - Syt9

DKO mice as compared to the Syt2 KO mice alone (Fig. 3J, K), and the amplitude of the presynaptic Ca^{2+} current was unchanged (not shown). Similarly as in the P1 - P2 data set, the mEPSC frequency was higher in the Syt9 - Syt2 DKO mice as compared to Syt2 KO, but this difference did not reach statistical significance (Fig. 3I; $p = 0.0617$). These results suggest that Syt9 is not a Ca^{2+} sensor for release at the early postnatal calyx synapse, but a small clamping role of Syt9 remains possible (see Discussion).

Syt1 drives a majority of fast release at pre-calyceal synapses

Because Syt9 is not the Ca^{2+} sensor at the immature calyx synapse, we next considered the possibility that Syt1 could represent the early Ca^{2+} sensor. Indeed, Syt1 mRNA is expressed in hindbrain around birth (Berton et al., 1997). To investigate Syt1 function at a mouse brain synapse *in-situ*, it was necessary to use conditional genetic deletion of Syt1, since constitutive inactivation of Syt1 leads to perinatal lethality (Geppert et al., 1994). We identified a novel floxed Syt1 mouse line (Fig. 4A; see Experimental Procedures), which we crossed with the Krox20Cre driver line (Voiculescu et al., 2000), to create a Syt1 conditional KO (cKO) mouse specific for the auditory brainstem (Maricich et al., 2009; Han et al., 2011).

We first recorded fiber-stimulation evoked EPSCs in MNTB neurons from Syt1 cKO mice and their control littermate mice at P2. This revealed a clear role for Syt1 for phasic AP-evoked release early postnatally. The EPSC amplitude was significantly smaller, and the rise time of EPSCs was prolonged in Syt1 cKO mice as compared to littermate control mice (Fig. 4B - D). Furthermore, the EPSCs in Syt1 cKO mice were visibly asynchronous (Fig. 4C). To confirm this observation quantitatively, we first calculated the integral of the EPSCs, which was significantly smaller in Syt1 cKO mice (Fig. 5E1; F). We then analyzed the half-maximal rise time of the normalized charge transfer curves, which revealed a significant rightward shift, thus demonstrating the more asynchronous release quantitatively (Fig. 4E2, G). The

mEPSC frequency was slightly, but significantly lower in Syt1 cKO mice as compared to control mice ($p < 0.05$; Fig. 4H); the mEPSC amplitude was unchanged (Fig. 4H). These findings strongly suggest that Syt1 is a Ca^{2+} sensor at pre-calyceal synapses early in development (P2), at a time when there is no detectable role for Syt2 (see Fig. 1). However, Syt1 did not suppress spontaneous release in the pre-calyceal synapses. This indicates that another release clamping mechanism, maybe in part contributed by Syt9, could act in recently developed synapses (see Discussion).

To further validate the role of Syt1 at the calyx of Held synapse early in development, we tested whether the protein is present at the calyx. Previous immunohistochemistry studies did not find detectable Syt1 proteins levels at the calyx of Held (Fox and Sanes, 2007; Sun et al., 2007; Xiao et al., 2010; Cooper and Gillespie, 2011). However, functionally relevant amounts of Syt1 protein might be present at low levels, but difficult to detect by immunofluorescence. We performed immunohistochemistry with an anti-Syt1 antibody in immature calyces at P5, using both control mice and the Syt1 cKO mice to validate the significance of low immunofluorescence signals. In control mice, many calyces identified by VGluT2 immunofluorescence showed a weak, but detectable Syt1 signal (see Fig. 5A1, A2; see arrows for examples). In contrast, in the Syt1 cKO littermate mouse at P5, we did not detect VGluT2 presynaptic profiles that showed a clearly identifiable Syt1 signal (Fig. 5B1, B2). To quantify these observations, we measured the Syt1 signal in VGluT2-positive calyceal profiles (see Supplemental Experimental Procedures). This revealed a significant reduction of Syt1 immunofluorescence in the Syt1 cKO mouse as compared to the control mouse (Fig. 5C; $p<0.001$, Kolmogorov-Smirnoff test).

The finding that the Syt1 immunofluorescence signal in immature calyces was weak does not reflect technical difficulties, or a weak specificity of the antibody. First, the observation that

the immunofluorescence signal was sensitive to genetic inactivation of Syt1 was repeated in another pair of wild-type and Syt1 cKO littermate mice with the same antibody (Fig. S4). Second, the presence of small punctae-like synapses with strong Syt1 signal (Fig. 5A1, B1), as well as the clear detection of Syt1 in rescue experiments by this antibody (see below; Fig. S5), validate the quality of the antibody and the immunohistochemistry protocols. Taken together, immunohistochemistry shows a low, but detectable Syt1 immunofluorescence in immature calces, which is sensitive to conditional removal of Syt1 protein.

Conditional Syt1 - Syt2 DKO calyces have abolished fast release

We found that Syt1 is responsible for a majority of phasic AP-evoked release at pre-calyceal synapses at P2 (Fig. 4), and there was a detectable Syt1 immunofluorescence signal in recently formed calyces at P5 (Fig. 5). The latter finding suggests that Syt1 continues to function in immature calyces, where it might mediate the fast release component which is insensitive to genetic deletion of Syt2 (Figs 2, 3). To investigate this possibility, it was necessary to create Syt1 - Syt2 conditional DKO mice (called cDKO mice below) . However, Syt1 - Syt2 cDKO mice, created by breeding $Syt1^{lox/lox}$, $Syt2^{+/-}$ and $Krox20^{+/Cre}$ mice, showed perinatal lethality (see Experimental Procedures). We therefore used virus-mediated Cre expression to recombine the floxed Syt1 locus in a spatially restricted manner in the VCN. An adenovirus driving the expression of both eGFP and Cre recombinase (Fig. 6A) was injected at P0 - P1 into the VCN of $Syt1^{lox/lox}$ / $Syt2^{-/-}$ mouse pups; a construct driving the expression of eGFP was sometimes used as a control. We then made paired recordings from immature calyx of Held synapses at P7. This age was chosen to allow for sufficient time for construct expression, while limiting the developmental down-regulation of the residual fast release seen in the Syt2 KO mice (see above; Fig. 2).

Using this approach, we found a significant contribution of Syt1 to the fast release component which remained in immature Syt2 KO calyces (Fig. 6B-D). In a control calyx of a Syt2 KO mouse (a non-infected calyx in a $Syt1^{lox/lox}$, $Syt2^{-/-}$ mouse injected with the Cre-expressing virus; Fig. 6B, white arrow), a vigorous fast release component was observed (Fig. 6C1, C2; black traces). Conversely, a recording from a neighboring GFP-positive calyx (thus, a Syt1 - Syt2 cDKO calyx; Fig. 6B, red arrow), showed a much smaller fast EPSC component, without apparent change of the presynaptic Ca^{2+} current (Fig. 6C1, red traces). Across all recordings, the peak EPSC amplitude, which is mainly caused by fast release, was reduced more than two-fold (Fig. 6D; $p < 0.001$), and the EPSC risetime was slightly prolonged (Fig. 6D; $p < 0.05$). However, the presynaptic Ca^{2+} current amplitudes and - kinetics were unchanged (Fig. 6E), nor was the Ca^{2+} current charge changed ($p = 0.64$; not shown). Deconvolution analysis revealed an ~ 3 fold lower peak release rate (Fig. 6C2, F) and ~3 fold smaller amplitude of the fast release component (Fig. 6C2, bottom; Fig. 6G). The number of vesicles released in the fast component was significantly reduced, while the time constant of the remaining fast release component was not changed significantly (Fig. 6H). Interestingly, the time constant of the slow release component increased from ~ 150 to ~ 300 ms in the Syt1 - Syt2 cDKO calyces (Fig. 6I), converging to the value of slow release observed in Syt2 KO mice at P13 - P15 (see above; Fig. 2C). This indicates that the "fast" Ca^{2+} sensors Syt1 and Syt2 also determine release speed from a slowly-releasable vesicle pool (Sakaba and Neher, 2001; see Discussion). On the other hand, neither the frequency, nor the amplitude of spontaneous mEPSCs were changed significantly in the Syt1 - Syt2 cDKO calyces (Fig. 6C3, J), suggesting that removal of Syt1 in the background of Syt2 KO mice does not further aggravate the release clamping phenotype.

Taken together, the results obtained with conditional genetic inactivation of Syt1 strongly suggest an expression change of Syt isoforms, with Syt1 being the more decisive Ca^{2+} sensor

early after birth, which is then downregulated and replaced by increasing amounts of Syt2 from about ~ P4 onwards.

Functional properties of Syt1, Syt2 and Syt9 as probed in a rescue approach

We finally wished to investigate the functional consequences of the Syt1 - Syt2 isoform switch at the calyx of Held synapse. For this purpose, we used a rescue approach, in which we re-expressed either Syt1 or Syt2 in mature Syt2 KO calyces (Kochubey and Schneggenburger, 2011). We also included Syt9 to validate whether this Syt isoform can, in principle, act as a Ca^{2+} sensor for release at a synapse *in-situ*.

Stereotactic injections of adenoviral vectors were made at P6 into the VCN of Syt2 KO mice (Experimental Procedures). Paired pre- and postsynaptic recordings were performed seven to eight days later (at P13 - P15) to allow for sufficient time for protein expression and for the full development of the Syt2 KO phenotype. Control recordings in Syt2 KO mice at P13 - P15 showed, as expected, exceedingly slow and small EPSCs (Fig. 7A). Rescue with the Syt1 and Syt2 constructs led to the re-appearance of large (~ 30 nA), and fast-rising EPSCs in response to presynaptic pool-depleting stimuli (Fig. 7B, C). These EPSCs were significantly, about fifteen-fold larger than those of Syt2 KO controls ($p < 0.001$; Fig. 7E). Re-expression of Syt9 led to a partial rescue with EPSC amplitudes of about 15 nA (Fig. 7D, E). The amplitude of mEPSCs, and the presynaptic Ca^{2+} currents were unchanged across all four groups (Fig. 7F, G). These results suggest that re-expression of Syt1 or Syt2 rescues the Ca^{2+} sensitivity of vesicle fusion, without acting via a change in quantal amplitude or presynaptic Ca^{2+} current amplitude.

We next performed a quantitative analysis of transmitter release rates and release time constants by deconvolving EPSCs, first concentrating on possible differences between Syt1

and Syt2 (Fig. 7H, I). Re-expression of Syt1 or Syt2 both rescued the fast- and the slow release component (Fig. 7B, C; middle), with time constants of ~ 1 - 1.5 ms and of ~ 20 - 30 ms (Fig. 7H, I). These parameters, and the amount of vesicles released in the fast- and in the slow component were not significantly different for Syt1 versus Syt2 rescue (Fig. 7H, I). The mEPSC frequency, which was elevated to ~ 35 Hz in Syt2 KO synapses, was reduced to ~ 3 Hz by Syt2 re-expression; this clamping effect was slightly smaller upon Syt1 re-expression (~5 Hz; Fig. 7J), but this difference was not statistically significant ($p = 0.24$). Taken together, the kinetic parameters of fast release and the number of released vesicles seemed indistinguishable between Syt1 and Syt2 rescue.

We finally also analyzed the rescue efficiency of Syt9. A previous paper showed that Syt9 could rescue the fast release deficit of cultured synapses from Syt1 KO mice albeit with slower kinetics (Xu et al., 2007); however, another report did not observe rescue activity of Syt9 (Dean et al., 2012). Therefore, our data obtained in a different system might help reconcile previous differences. In Syt9 rescue experiments, we found clear rescue activity in all but one of the recorded GFP-positive calyces (n = 23 / 24 recordings). However, EPSC amplitudes in response to pool-depleting presynaptic depolarizations were about two-fold smaller upon rescue with Syt9 as compared to Syt1 and Syt2 ($p < 0.01$ and 0.001; see Fig. 7E), and EPSC risetimes were slower. Deconvolution analysis showed a fast release time constant of ~ 2.5 ms upon Syt9 rescue, significantly slower than rescue with Syt1 (Fig. 7 H). Similarly, fewer vesicles were released in both the fast- and the slow release component upon Syt9 rescue as compared to rescue with Syt1 and Syt2, but these differences only reached statistical significance for the comparison of A_{fast} with Syt1, and A_{slow} with Syt2 (Fig. 7H, I). In immunohistochemical experiments with the Myc-tagged Syt9 construct and also using an anti-Syt9 antibody, recombinant Syt9 protein was clearly present in transduced (GFP-positive) calyces of Held, but a lower expression density as compared to the recombinant Syt1

protein cannot be excluded at present (Fig. S5). Thus, rescue experiments suggest that Syt9 can, in principle, act as a Ca^{2+} sensor for fast release (Xu et al., 2007), but it remains possible that Syt9 is targeted less efficiently to presynaptic nerve terminals (Dean et al., 2012).

Discussion

Using mouse genetics, immunohistochemistry, virus-mediated transgenesis at specific synapses and electrophysiological recordings, we show that synaptic transmission at a developing hindbrain synapse depends on Syt1 early postnatally, but later switches to Syt2. Despite detectable expression of Syt9 and the ability of this isoform to rescue fast release at least partially, genetic deletion of Syt9 did not show a role of this isoform as a Ca^{2+} sensor early postnatally. Thus, our data reveal a developmental Syt1 to Syt2 isoform switch at an identified CNS synapse. This developmental isoform switch might influence release probability or presynaptic plasticity, although rescue experiments revealed only subtle differences in the release kinetics between Syt1 and Syt2. Our analysis also suggests that the expression levels of Syt1 and/or Syt2 determine the intrinsic speed of transmitter release.

Previous work showed that Syt2 is expressed in hindbrain areas (Berton et al., 1997; Pang et al., 2006a) and that genetic deletion of Syt2 abolishes fast release at the calyx of Held synapse (Sun et al., 2007; Kochubey and Schneggenburger, 2011). Nevertheless, given the central role of hindbrain areas in breathing, feeding and autonomic control of body functions (Kandel et al., 2013), it remained puzzling that Syt2 KO mice survive until ~ 2 weeks, if Syt2 should be the only fast Ca^{2+} sensor at most hindbrain and spinal cord synapses. Our study offers an explanation for this conundrum, by showing that release at a large hindbrain synapse, the calyx of Held, does in fact *not* depend on Syt2 early postnatally, but rather, on Syt1. This result was initially surprising given that Syt1 was previously not detected in the calyx (Pang et al., 2006b; Fox and Sanes, 2007; Sun et al., 2007; Xiao et al., 2010; Cooper and Gillespie,

2011). However, we found a weak Syt1 immunofluorescence signal in immature calyces, which was sensitive to genetic inactivation of Syt1 (Fig. 5). A role of Syt1 as a fast Ca^{2+} sensor early postnatally in hindbrain is consistent with a developmental expression study, which found that Syt1 mRNA is present in many brain areas (including the hindbrain) already at birth, whereas Syt2 was more limited to hindbrain and midbrain and had a delayed expression onset (Berton et al., 1997). A previous study found partially reduced release at the NMJ of Syt2 KO mice, but the Ca^{2+} sensor of the remaining fast release was not identified (Pang et al., 2006a). Taken together, a picture emerges in which transmitter release at hindbrain synapses initially depends on Syt1, whereas Syt2 has a delayed expression onset by a few days, and then replaces Syt1.

We used a novel floxed allele to study the role of Syt1 for transmitter release "*in-situ*", that is, at synapses formed in the developing mouse brain. Because of perinatal lethality, studies with the conventional Syt1 KO mice have been limited to cultured neurons (Geppert et al., 1994; Nishiki and Augustine, 2004; Maximov and Südhof, 2005; Kerr et al., 2008). Interestingly, it is possible that the perinatal lethality of conventional Syt1 KO mice largely results from the requirement of Syt1 at hindbrain synapses early postnatally, which we have uncovered here for the calyx synapse. In a previous study, the role of Syt1 for GABA release from hippocampal basket cells was studied; lethality was circumvented by using organotypic cultures. Only a small contribution of Syt1 to phasic GABA release was found, which suggested a primary role of another, non-identified Ca^{2+} sensor (Kerr et al., 2008). There is immunohistochemical evidence for the expression of Syt2 at GABAergic terminals of Parvalbumin (PV) - expressing interneurons, and Syt2 expression is developmentally upregulated in these cells (Okaty et al., 2009; Garcia-Junco-Clemente et al., 2010; Sommeijer and Levelt, 2012). Thus, an isoform switch towards Syt2 could also occur in PV-interneurons, but this possibility has yet to be demonstrated functionally. The transcriptional regulatory

networks which control the expression of Syt1 and Syt2 are beginning to be investigated (Pang et al., 2010; Lucas et al., 2014), but more work is clearly needed to establish these mechanisms.

We initially suspected that Syt9 could be a Ca^{2+} sensor early postnatally, because this isoform is expressed early-on but then downregulated with further development (Fig. 3; Xiao et al., 2010). We found that Syt9 rescued the strong release phenotype of mature Syt2 KO calyces at least partially, thus confirming and extending a previous study in cultured neurons (Xu et al., 2007). However, genetic deletion did not reveal a function of Syt9 as a Ca^{2+} sensor for release at the immature calyx (Fig. 3). It is possible, however, that Syt9 contributes to release clamping in synapses of young mice, because mEPSC frequencies were slightly increased in two independent data sets obtained in young mice (Fig. 3). A previous study showed that Syt9 KO reduced phasic GABA release in cultured striatal neurons (Xu et al., 2007), but our study did not reveal a role of Syt9 in Ca^{2+} - evoked release. Overall, the physiological role of Syt9 needs further investigation. Syt9 was found more strongly expressed in hypothalamus, accumbens, striatum and olfactory bulb (Xu et al., 2007; Allen Brain Atlas) and thus could function more specifically in these brain areas.

Is there a functional advantage for hindbrain synapses, or in general, for fast-releasing synapses to switch their expression from Syt1 to Syt2? Using virus-mediated rescue of the Syt2 release phenotype at mature calyces, we found that the release kinetics conferred by Syt1 and Syt2 were not significantly different (Fig. 7). This finding does not agree with a rescue study in cultured Syt1 KO neurons, which found significantly faster synaptic currents following rescue by Syt2 as compared to Syt1 (Xu et al., 2007). On the other hand, Syt2 rescue in chromaffin cells led to slower release than rescue with Syt1 (Nagy et al., 2006). Also, a previous *in-vitro* study found slightly faster disassembly kinetics for Syt1 as compared

to Syt2 (Hui et al., 2005). Therefore, the view that Syt2 confers faster release kinetics than Syt1 (Xu et al., 2007) is not justified by our data nor by other previous studies. However, it remains possible that in the cortical inhibitory synapses used in the rescue experiments of Xu et al. (2007), Syt2 indeed confers faster release than Syt1.

Although we did not observe differences in the release kinetics between Syt1 and Syt2 at the calyx of Held (Fig. 7), other functional differences between the two isoforms might contribute to the biological significance of the isoform switch. Thus, Syt1 contains a phosphorylation site for CaMKII and PKC which is absent in Syt2 (Hilfiker et al., 1999; Nagy et al., 2006). The function of this site in presynaptic plasticity has not been investigated, but it is conceivable that Syt2 confers a release machinery with less presynaptic plasticity and/or modulation, which might be advantageous for more reliable information transfer at fast-releasing synapses. A differential activity of Syt1 versus Syt2 in supporting vesicle endocytosis might be envisaged, although there are no indications yet for possible differential binding activities of Syt1 and Syt2 to endocytic adapter proteins like AP-2 or stonin-2 (Ullrich et al., 1994; Martina et al., 2001). Also, there are other presynaptic proteins that undergo a developmental expression change at the calyx synapse, including the Ca^{2+} channel α subunits (Iwasaki and Takahashi, 1998), the filamentous protein Septin-5 (Yang et al., 2010), and Complexin1 and -2 isoforms (Chang et al., 2015). Therefore, it is possible that molecular interaction partners that are specific for a given developmental stage act in concert, and further optimize the function of Syt2 expressed at the more mature calyx of Held synapse.

Our study also allows us to draw conclusions on the mechanisms which can regulate the *intrinsic* kinetics of transmitter release, that is, the release kinetics at a given increase in intracellular Ca^{2+} concentration (Wölfel et al., 2007). In the complete absence of Syt1 and Syt2 (in Syt2 KO mice at ~ P14), release evoked by Ca^{2+} uncaging and by presynaptic

depolarization was excessively slow (~ 250 - 300 ms; Figs 2, 7). In addition, the speed of both the fast- and the slow release component were slowed in immature Syt2 KO mice, in which only low levels of Syt1 remained (Fig. 2). Re-expression of either Syt1 or Syt2 effectively re-established both the fast- and the slow release component and their kinetics (Fig. 7). Thus, both release components depended on Syt1 or Syt2; this is different from chromaffin cells, where Syt1 deletion more selectively reduced the fast component (Voets et al., 2001). More generally, the modulation of release speed by the expression level of residual Syt1 suggests that the intrinsic speed of release is a function of the Syt1 (or Syt2) abundance at the release machinery. This conclusion is analogous to the results found with titrated expression of SNAP-25 in chromaffin cells (Mohrmann et al., 2010). Thus, the expression strength, and the copy number of Syt1/2 proteins or SNARE proteins could contribute to determining the intrinsic speed and probability of transmitter release in a synapse.

Experimental Procedures

Ethics statement

All procedures of mouse breeding, handling, surgery and sacrifice for slice electrophysiology and immunohistochemistry were approved by the Veterinary office of the Canton of Vaud, Switzerland (authorizations 1880, 2063).

Synaptotagmin KO mouse lines

The Syt2 KO mouse line (RRID:MGI_3696550) was the same as described originally in (Pang et al., 2006a); these mice were elevated in heterozygous breeding. The $Syt9^{-/-}$ mice were originally described by Xu et al. (2007) and purchased from Jackson labs (B6;129-$Syt5^{tm2Sud}$; RRID:MGI_3715455). However, in the previous breeding history a cross with an ubiquitous Cre carrier took place, thus the Syt9 line used here was a conventional KO.

For the experiments with conditional Syt1 KO mice, we identified a floxed Syt1 mutant line $Syt1^{tm1a(EUCOMM)Wtsi}$ at the European Mouse Mutant Archive (EMMA, Monterotondo, Italy; EM06829; RRID:MGI_5450372; see Skarnes et al., 2011 for the general design of the floxed lines). For further details of the re-derivation of the Syt1lox mice, and for breeding and genotyping procedures of all mouse lines, see Supplementary Experimental Procedures for Synaptotagmin mouse lines.

Adenovirus vectors and stereotactic surgery

For Cre-expression for conditional removal of the floxed Syt1 allele (Fig. 6), we used a second generation adenoviral vector (Ad: HSyn1: eGFP - IRES - Cre), which was injected stereotaxically into VCN of newborn mice at P0/P1 (see also Genç et al., 2014). For the Syt1, Syt2, and Syt9 rescue experiments in calyces of Held of Syt2 KO mice, we used the same second generation adenoviral vector, which now drove the expression of GFP and either one

of the three Myc-tagged Syts (Ad: HSyn1 - eGFP : HSyn1 - MycSyt1/2/9); stereotaxic injections were made at P6 into the VCN (Kochubey and Schneggenburger, 2011). Details for the preparation of adenovirus vectors, and for stereotaxic injections can be found in Supplementary Experimental Procedures for viral vectors and stereotaxic surgery.

Slice electrophysiology

Whole-cell patch-clamp recordings were made from MNTB neurons, or in double recordings of MNTB neurons and their presynaptic calyx of Held, using 200 µm thick native brainstem slices (Kochubey and Schneggenburger, 2011). Details on the slicing procedures, electrophysiological measurements, Ca^{2+} uncaging, and electrophysiological data analysis can be found in Supplemental Experimental Procedures for Slice electrophysiology and Ca^{2+} uncaging.

qPCR, Immunohistochemistry and Western blot analysis

The protocols for qPCR analysis, for immunohistochemistry and image analysis, and for Western blot analysis are given in Supplemental Experimental Procedures for qPCR, immunohistochemistry, and Western blot.

Statistical analysis

Statistical significance was assessed with a two-tailed Student's t-test, or using Kolmogorov-Smirnov test when indicated. Significance levels are indicated in bar graph summary plots according to the convention: * $p < 0.05$, ** $p < 0.01$, *** $p < 0.001$. Error bars indicate the standard error of the mean (S.E.M.).

Author Contributions

Conceptualization, O.K. and R.S.; Investigation, O.K. and N.B.; Formal Analysis, O.K. and N.B.; Writing – Original Draft, O.K. and R.S.; Writing – Review & Editing, O.K., N.B. and R.S.; Funding Acquisition, R.S.

Acknowledgements

We thank Dr. Thomas Südhof for Syt2 mutant mice, Dr. Isabelle Barde for the help in IVF re-derivation of Syt1^{floxed} mice, Dr. Graham Knott for expert help in EM experiments, and Heather Murray and Jessica Dupasquier for excellent technical assistance. Confocal imaging was done at the Bioimaging and Optics Platform at EPFL. The work was supported by grants from the Swiss National Science Foundation (SNSF 310030B_156934 / 1) and the Deutsche Forschungsgemeinschaft (SPP 1608 - SCHN 451/5-1).

Figure legends

Figure 1. Fast Syt2-independent neurotransmission at the developing calyx of Held synapse.

(**A**) A schematic representation of the developmental stages investigated in this study: pre-calyceal glutamatergic synapses at P1 - P3, immature giant calyx terminals at P4 - P7, and the mature calyx of Held synapse at P13 - P15.

(**B, C**) Top: individual example EPSC traces (grey) and the average of five EPSCs (black) evoked by maximal afferent fiber stimulation in a wild-type control (B) and a Syt2 KO mouse (C) at P2 - P3. Bottom: examples of mEPSC traces recorded from the same cells.

(**D, E**) Summary plots of peak EPSC amplitudes and 20-80% EPSC risetimes (D), and of mEPSC frequencies and amplitudes (E) at P2 - P3. Here and in subsequent panels, grey and red color codes are used for control and Syt2 KO, respectively.

(**F, G**) Similar experiment as in (B, C) but performed in a $Syt2^{+/+}$ control mouse (F) and Syt2 KO mouse (G) at P5 - P6. The average EPSC trace in blue (G) is shown at the same scale as the control. Bottom: example mEPSC traces.

(**H, I**) Summary plots of peak EPSC amplitudes and risetimes (H), and of mEPSC frequencies and amplitudes (I) at P5 - P6.

(**J**) Example confocal images of VGluT2 and Syt2 immunofluorescence in the MNTB of P0, P2 and P5 wild-type mice (J1). The white boxes mark the areas displayed at higher magnification in (J2). Note the very low or absent Syt2 signal in VGluT2-positive, putative pre-calyceal terminals at P0 and P2, followed by strong Syt2 expression in immature calyces at P5. Scale bars are 10 and 2 μm in (J1) and (J2), respectively.

Error bars represent SEM. See also Fig. S1.

Figure 2. Developmental progression of the release phenotype in Syt2 KO mice analyzed with presynaptic Ca^{2+} uncaging.

(**A**) Example pre- and postsynaptic paired recordings with presynaptic Ca^{2+}-uncaging performed in immature Syt2 KO calyces at P5 - P6. Panels from top to bottom show: Presynaptic $[Ca^{2+}]_i$ steps induced by Ca^{2+} uncaging (A1, top); corresponding color-coded EPSC traces (A1, bottom); release rates (A2, top) and integrated release rates (cumulative release, A2, bottom); example mEPSC traces recorded in the same cell (A3). Overlaid green dashed line in (A2) shows the double-exponential fit of cumulative release to assess the release time constants.

(**B**) Same experiment as in (A), performed in a Syt2 KO calyx from an intermediate age group (P8 - P10). Note the different vertical scale bars.

(**C**) Same experiment as in (A, B), performed in a mature Syt2 KO calyx in the P13 - P15 group. Note that a single exponential was sufficient to fit the cumulative release trace (C2).

(**D**) Summary plot of the peak release rates measured in Syt2 KO mice at the indicated three age groups.

(**E, F**) Summary plots of the fast- and slow release time constants (E), and the corresponding amplitudes of the fit components (F) at the three developmental stages. Each symbol represents the largest recorded flash response (for $[Ca^{2+}]_i > 10\ \mu M$) in a given synapse. Two cells with exceedingly slow release kinetics were excluded from the analysis.

(**G**) Summary plot of the mEPSC frequency at three developmental stages of Syt2 KO synapses.

(**H, I**) Peak release rates (H) and release delays (I) plotted as a function of post-flash $[Ca^{2+}]_i$ in Syt2 KO synapses at two age groups (P5 - P6, black symbols; P13 - P15, grey symbols. Solid lines are linear fits through the data in log-log space; the fit slopes of the release rate data assess the intrinsic Ca^{2+} cooperativity of release. Note that the data obtained in Syt2 KO mice at P13 - P15 (open grey points) are the same as shown in Fig. 4 of Babai et al. (2014).

Error bars represent SEM. See also Fig. S2.

Figure 3. Syt9 is not a Ca^{2+} sensor at pre-calyceal and immature calyx synapses.

(**A**) Expression of Syt1, -2 and -9 mRNA relative to β-actin for mRNA harvested from the cochlear nucleus at the indicated postnatal day. Relative ΔCt values are averages of three replicates.

(**B**) Western blot analysis of the Syt9 expression in the brain of control ($Syt9^{+/+}$) and Syt9 KO mice to validate protein removal of Syt9 in the mutant. OB – olfactory bulb; BS – brainstem at the level of superior olive; CTX – neocortex; E2T – ET2 cells expressing Syt9.

(**C, D**) Top: five consequent EPSCs (grey) and the average traces (black) evoked by maximal afferent fiber stimulation in the MNTB of a P1 - P2 Syt9 control mouse (C), and in a Syt9 KO mouse (D). Bottom: mEPSC traces recorded from the same cells.

(**E, F**) Summary plots of EPSC amplitudes and risetimes (E), and of mEPSC frequency and -amplitude (F) from the measurements of $Syt9^{+/+}$ mice (called Syt9 ctrl) and Syt9 KO mice at P1 - P2.

(**G**) Example paired pre- and postsynaptic recordings at a calyx of Held synapse from a Syt2-Syt9 DKO mouse at P6. From top to bottom: presynaptic voltage-clamp protocol; presynaptic Ca^{2+}-current; EPSC; release rate trace obtained by EPSC deconvolution; cumulative release rate trace with the double-exponential fit line overlaid in grey; example mEPSC trace from the same cell. Note the prominent fast release component despite the absence of Syt9 and Syt2.

(**H, I**) Summary plots of EPSC amplitude and risetimes (H), and of mEPSC frequencies (I) measured in Syt2 KO - and Syt2 - Syt9 DKO mice in paired pre- and postsynaptic recordings at P5 - P6.

(**J, K**) Summary plots of the time constants and amplitudes of the fast (J) and the slow (K) release components, measured in Syt2 KO and Syt2-Syt9 DKO calyces at P6 - P8.
Error bars represent SEM. See also Fig. S3.

Figure 4. AP-evoked release at pre-calyceal synapses requires Syt1.

(**A**) A scheme of the design of floxed Syt1 mice obtained from EMMA (Skarnes et al., 2011). Mice carrying the $Syt1^{floxed}$ allele (top; Syt1 exons shown in yellow) were first crossed with a generic FLP recombinase carrier, and consequently with $Krox20^{Cre}$ mice to produce Syt1 cKO mice specific for auditory brainstem (see Experimental Procedures).

(**B, C**) Top: five consecutive EPSC traces (grey and pink), and the resulting average EPSC (black and red) evoked by maximal afferent fiber stimulation in a $Syt1^{lox/+}$ mouse (Syt1 control; B) and in a Syt1 cKO mice (C) at P2. Bottom: Example mEPSC traces from the same cells.

(**D**) Summary plot of EPSC amplitudes (left) and 20 - 80% EPSC risetimes (right) in Syt1 control mice and in Syt1 cKO mice.

(**E**) Cumulative charge analysis of single AP-evoked EPSCs in individual recordings of Syt1 control mice (gray traces) and of Syt1 cKO mice (E1, grey and pink traces, respectively). Each grey and pink cumulative EPSC trace is a representative record from a single neuron; red and black traces are the averages across cells. In (E2), the Q_{EPSC} traces are normalized to the total charge transfer at 300 ms after the stimulation. The average latencies to 50% cumulative charge are marked by the dashed vertical lines.

(**F, G**) Summary plots of the cumulative EPSC charge at 300 ms (F), and of the latencies to 50% of that charge (G; see also E2), measured from Syt1 control and Syt1 cKO mice at P2. Note the significantly smaller Q_{EPSC} value ($p < 0.01$), and the significantly longer latency ($p < 0.001$) in Syt1 cKO mice as compared to Syt1 control mice.

(**H**) Summary plots of mEPSC frequency (left) and mEPSC amplitude (right) in each genotype.

Error bars represent SEM.

Figure 5. Low but detectable levels of Syt1 protein in immature calyces of Held terminals.

(**A**) A confocal images of MNTB after immunostaining against VGluT2 (green channel) and Syt1 (red) in a Syt1 control mouse at P5 (A1). Many VGluT2-positive presynaptic profiles also expressed visually discernable Syt1 signal (A1, arrows show example calyces). In some calyces, the Syt1 signal was not apparent (arrowheads). The calyces highlighted by arrows are shown in higher magnification in A2.

(**B**) Confocal analysis as in (A), but from a littermate Syt1 cKO ($Syt1^{lox/lox}$, $Krox20^{Cre}$) mouse at P5. Imaging was done in parallel to the control sections (A) with identical microscope settings. Note the absence of Syt1-postive calyceal presynaptic profiles (arrowheads; example terminals are shown expanded in B2). Small, more intensely stained Syt1 puncta remained, which must originate from neurons outside of the Krox20 domain. Scale bars are 10 μm and 2 μm in (A1, B1) and (A2, B2), respectively.

(**C**) Histograms and cumulative frequency plots of the local background-corrected Syt1 immunofluorescence measured in the Syt1 control - and Syt1 cKO mice at P5 (see Supplemental Experimental Procedures).

See also Fig. S4

Figure 6. A fast release component resistant to Syt2 deletion depends on Syt1.

(**A**) Schematic of an adenoviral vector used to co-express Cre recombinase and eGFP.

(**B**) Transmission - (*left*) and fluorescent eGFP images (*right*) of an adjacent non-infected control calyx (white arrow), and a Cre - expressing calyx (red arrow) in a slice from a $Syt1^{lox/lox}$ / Syt2 KO mouse at P7. Scale bars are 10 μm.

(**C**) Paired recordings from the two neighboring calyx synapses shown in (A). Black and red traces show the recording from the Syt2 KO (control calyx) and from the Syt1 - Syt2 cDKO calyx. Panels from top to bottom: presynaptic voltage clamp protocol, presynaptic Ca^{2+}-currents, EPSCs (C1); release rate traces, cumulative release traces (C2); example mEPSC traces recorded from the same cells (C3). The blue lines in the lower panel of C2 are the fits with double-exponential plus line functions.

(**D, E**) Summary plots of the EPSC amplitudes (D, left), the 20-80% risetimes of EPSCs (D, right), and of the presynaptic Ca^{2+} current amplitude (E, left) and the Ca^{2+} current risetime (E, right). Note the significant changes in the EPSC amplitudes ($p < 0.001$) and EPSC risetimes ($p < 0.05$) despite unchanged presynaptic Ca^{2+} currents.

(**F**) Summary plot of peak release rates measured in Syt2 KO calyces (control group) and in Syt1 - Syt2 cDKO synapses at P7.

(**G**) Cumulative release traces from individual recordings (grey and pink traces), and averages of cumulative release traces across all recorded cells (thick black and red lines). Note the smaller fast release component in most recordings from Syt1 - Syt2 cDKO calyces.

(**H, I**) Summary plots of release time constants (*left*) and of the corresponding number of released vesicles in each kinetic component (*right*). Note the significantly smaller fast release component ($p < 0.001$), and the significant slowing of the slow component ($p < 0.01$) in Syt1 - Syt2 cDKO calyx synapses.

(**J**) Summary plots of the mEPSC frequencies (left) and of the mEPSC amplitudes (right) in Syt2 KO calyces and Syt1-Syt2 cDKO calyces.

Error bars represent SEM.

Figure 7. Comparative rescue of the Syt2 release phenotype at mature calyces reveals functional properties of Syt1, Syt2 and Syt9.

In these rescue experiments, adenoviral particles driving the expression of MycSyt1/2/9 were injected into the VCN of Syt2 KO mice at P6, and paired pre- and postsynaptic recordings were made at P13 - P15.

(**A**) Paired recordings from a non-injected Syt2 KO mouse at P14. From top to bottom: presynaptic Ca^{2+}-currents evoked by step depolarization to 0 mV for 50 ms; EPSC (note expanded scale for the grey trace); cumulative release trace with overlaid single exponential fit in red; example mEPSC traces.

(**B-D**) Similar experiments as in (A), but in calyces of Held rescued with either Syt1 (B; a P13 mouse), Syt2 (C; a P13 mouse) or Syt9 (D; a P13 mouse). The insets show the rising phase of the EPSCs, with the 20-80% risetimes indicated by arrowheads. Double exponential plus line functions (red lines) were required to fit cumulative release traces.

(**E-J**) Summary plots of all analyzed parameters from the rescue experiments; the rescue construct used is indicated by the color code on the left. Significant differences between groups are indicated by a bracket, with star symbols indicating the degree of significance (see Experimental Procedures); no bracket indicates no statistical significance ($p > 0.05$). The individually analyzed parameters were: peak EPSC amplitudes and EPSC rise times (E); mEPSC amplitudes (F); presynaptic Ca^{2+} current amplitudes (G); fast release time constants and number of vesicles released in the fast component (H); slow release time constants and number of vesicles released in the slow component (I); and mEPSC frequency (J). Note that the Syt2 KO synapses showed no fast release component.

Error bars represent SEM. See also Fig. S5.

References

Allen Mouse Brain Atlas [Internet] Website © 2015 Allen Institute for Brain Science. Available from: http://mouse.brain-map.org

Babai, N., Kochubey, O., Keller, D., and Schneggenburger, R. (2014). An alien divalent ion reveals a major role for Ca^{2+} buffering in controlling slow transmitter release. J. Neurosci. *34*, 12622-12635.

Berton, F., Iborra, C., Boudier, J.A., Seagar, M.J., and Marquèze, B. (1997). Developmental regulation of synaptotagmin I, II, III, and IV mRNAs in the rat CNS. J. Neurosci. *17*, 1206-1216.

Bollmann, J., Sakmann, B., and Borst, J. (2000). Calcium sensitivity of glutamate release in a calyx-type terminal. Science *289*, 953-957.

Borst, J.G., and Soria van Hoeve, J. (2012). The calyx of Held synapse: from model synapse to auditory relay. Annu. Rev. Physiol. *74*, 199-224.

Cao, P., Maximov, A., and Südhof, T.C. (2011). Activity-dependent IGF-1 exocytosis is controlled by the Ca^{2+}-sensor synaptotagmin-10. Cell *145*, 300-311.

Chang, S., Reim, K., Pedersen, M., Neher, E., Brose, N., and Taschenberger, H. (2015). Complexin stabilizes newly primed synaptic vesicles and prevents their premature fusion at the mouse calyx of Held synapse. J. Neurosci. *35*, 8272-8290.

Cooper, A.P., and Gillespie, D.C. (2011). Synaptotagmins I and II in the developing rat auditory brainstem: Synaptotagmin I is transiently expressed in glutamate-releasing immature inhibitory terminals. J. Comp. Neurol. *519*, 2417-2433.

Craxton, M. (2010). A manual collection of Syt, Esyt, Rph3a, Rph3al, Doc2, and Dblc2 genes from 46 metazoan genomes--an open access resource for neuroscience and evolutionary biology. BMC genomics *11*, 37.

de Wit, H., Walter, A.M., Milosevic, I., Gulyas-Kovacs, A., Riedel, D., Sorensen, J.B., and Verhage, M. (2009). Synaptotagmin-1 docks secretory vesicles to syntaxin-1/SNAP-25 acceptor complexes. Cell *138*, 935-946.

Dean, C., Dunning, F.M., Liu, H., Bomba-Warczak, E., Martens, H., Bharat, V., Ahmed, S., and Chapman, E.R. (2012). Axonal and dendritic synaptotagmin isoforms revealed by a pHluorin-syt functional screen. Mol. Biol. Cell *23*, 1715-1727.

Fedchyshyn, M.J., and Wang, L.-Y. (2005). Developmental transformation of the release modality at the calyx of Held synapse. J. Neurosci. *25*, 4131-4140.

Fernández-Chacón, R., Konigstorfer, A., Gerber, S.H., Garcia, J., Matos, M.F., Stevens, C.F., Brose, N., Rizo, J., Rosenmund, C., and Südhof, T.C. (2001). Synaptotagmin I functions as a calcium regulator of release probability. Nature *410*, 41-49.

Fox, M.A., and Sanes, J.R. (2007). Synaptotagmin I and II are present in distinct subsets of central synapses. J. Comp. Neurol. *503*, 280-296.

Garcia-Junco-Clemente, P., Cantero, G., Gomez-Sanchez, L., Linares-Clemente, P., Martinez-Lopez, J.A., Lujan, R., and Fernández-Chacón, R. (2010). Cysteine string protein-α prevents activity-dependent degeneration in GABAergic synapses. J. Neurosci. *30*, 7377-7391.

Genç, Ö., Kochubey, O., Toonen, R.F., Verhage, M., and Schneggenburger, R. (2014). Munc18-1 is a dynamically regulated PKC target during short-term enhancement of transmitter release. eLife *3:e01715*.

Geppert, M., Archer, B.T., 3rd, and Südhof, T.C. (1991). Synaptotagmin II. A novel differentially distributed form of synaptotagmin. J. Biol. Chem. *266*, 13548-13552.

Geppert, M., Goda, Y., Hammer, R.E., Li, C., Rosahl, T.W., Stevens, C.F., and Südhof, T.C. (1994). Synaptotagmin I: a major Ca^{2+} sensor for transmitter release at a central synapse. Cell *79*, 717-727.

Goda, Y., and Stevens, C.F. (1994). Two components of transmitter release at a central synapse. Proc. Natl. Acad. Sci. USA *91*, 12942-12946.

Han, Y., Kaeser, P.S., Südhof, T.C., and Schneggenburger, R. (2011). RIM determines Ca^{2+} channel density and vesicle docking at the presynaptic active zone. Neuron *69*, 304-316.

Heidelberger, R., Heinemann, C., Neher, E., and Matthews, G. (1994). Calcium dependence of the rate of exocytosis in a synaptic terminal. Nature *371*, 513-515.

Heinemann, C., Chow, R.H., Neher, E., and Zucker, R.S. (1994). Kinetics of the secretory response in bovine chromaffin cells following flash photolysis of caged Ca^{2+}. Biophys. J. *67*, 2546-2557.

Hilfiker, S., Pieribone, V.A., Norstedt, C., Greengard, P., and Czernik, A.J. (1999). Regulation of synaptotagmin I phoshorylation by multiple protein kinases. J. Neurochem. *73*, 921-932.

Hoffpauir, B.K., Grimes, J.L., Mathers, P.H., and Spirou, G.A. (2006). Synaptogenesis of the calyx of Held: Rapid onset of function and one-to-one morphological innervation. J. Neurosci. *26*, 5511-5523.

Hoffpauir, B.K., Kolson, D.R., Mathers, P.H., and Spirou, G.A. (2010). Maturation of synaptic partners: functional phenotype and synaptic organization tuned in synchrony. J. Physiol. *588*, 4365-4385.

Hui, E., Bai, J., Wang, P., Sugimori, M., Llinas, R.R., and Chapman, E.R. (2005). Three distinct kinetics groupings of the synaptotagmin family: Candidate sensors for rapid and delayed exocytosis. Proc. Natl. Acad. Sci. USA *102*, 5210-5214.

Imig, C., Min, S.W., Krinner, S., Arancillo, M., Rosenmund, C., Südhof, T.C., Rhee, J., Brose, N., and Cooper, B.H. (2014). The morphological and molecular nature of synaptic vesicle priming at presynaptic active zones. Neuron *84*, 416-431.

Iwasaki, S., and Takahashi, T. (1998). Developmental changes in calcium channel types mediating synaptic transmission in rat auditory brainstem. J. Physiol. *509*, 419-423.

Kandel, E.R., Schwartz, J.H., Jessell, T.M., Siegelbaum, S.A., and Hudspeth, A.J. (2013). Principles of Neural Science. McGraw Hill.

Kerr, A.M., Reisinger, E., and Jonas, P. (2008). Differential dependence of phasic transmitter release on synaptotagmin 1 at GABAergic and glutamatergic hippocampal synapses. Proc. Natl. Acad. Sci. USA *105*, 15581-15586.

Kochubey, O., and Schneggenburger, R. (2011). Synaptotagmin increases the dynamic range of synapses by driving Ca^{2+} - evoked release and by clamping a near-linear remaining Ca^{2+} sensor. Neuron *69*, 736-748.

Leão, R.M., and von Gersdorff, H. (2009). Synaptic vesicle pool size, release probability and synaptic depression are sensitive to Ca^{2+} buffering capacity in the developing rat calyx of Held. Braz. J. Med. Biol. Res. *42*, 94-104.

Littleton, J.T., Stern, M., Schulze, K., Perin, M., and Bellen, H.J. (1993). Mutational analysis of Drosophila *synaptotagmin* demonstrates its essential role in Ca^{2+}-activated neurotransmitter release. Cell *74*, 1125-1134.

Lucas, E.K., Dougherty, S.E., McMeekin, L.J., Reid, C.S., Dobrunz, L.E., West, A.B., Hablitz, J.J., and Cowell, R.M. (2014). PGC-1α provides a transcriptional framework for synchronous neurotransmitter release from Parvalbumin-positive interneurons. J. Neurosci. *34*, 14375-14387.

Maricich, S.M., Xia, A., Mathes, E.L., Wang, V.Y., Oghalai, J.S., Fritzsch, B., and Zoghbi, H.Y. (2009). Atoh1-lineal neurons are required for hearing and for the survival of neurons in the spiral ganglion and brainstem accessory auditory nuclei. J. Neurosci. *29*, 11123-11133.

Marqueze, B., Boudier, J.A., Mizuta, M., Inagaki, N., Seino, S., and Seagar, M. (1995). Cellular localization of synaptotagmin I, II, and III mRNAs in the central nervous system and pituitary and adrenal glands of the rat. J.Neurosci. *15*, 4906-4917.

Martina, J.A., Bonangelino, C.J., Aguilar, R.C., and Bonifacino, J.S. (2001). Stonin 2: an adaptor-like protein that interacts with components of the endocytic machinery. J. Cell Biol. *153*, 1111-1120.

Maximov, A., and Südhof, T.C. (2005). Autonomous function of Synaptotagmin 1 in triggering synchronous release independent of asynchronous release. Neuron *48*, 547-554.

Mohrmann, R., de Wit, H., Verhage, M., Neher, E., and Sorensen, J.B. (2010). Fast vesicle fusion in living cells requires at least three SNARE complexes. Science *330*, 502-505.

Nagy, G., Kim, J.H., Pang, Z.P., Matti, U., Rettig, J., Südhof, T.C., and Sorensen, J.B. (2006). Different effects on fast exocytosis induced by synaptotagmin 1 and 2 isoforms and abundance but not by phosphorylation. J. Neurosci. *26*, 632-643.

Neher, E., and Sakaba, T. (2001). Combining deconvolution and noise analysis for the estimation of transmitter release rates at the calyx of Held. J. Neurosci. *21*, 444-461.

Nishiki, T., and Augustine, G. (2004). Synaptagmin I synchronizes transmitter release in mouse hippocampal neurons. J. Neurosci. *24*, 6127-6132.

Okaty, B.W., Miller, M.N., Sugino, K., Hempel, C.M., and Nelson, S.B. (2009). Transcriptional and electrophysiological maturation of neocortical fast-spiking GABAergic interneurons. J. Neurosci. *29*, 7040-7052.

Pang, Z.P., Melicoff, E., Padgett, D., Liu, Y., Teich, A.F., Dickey, B.F., Lin, W., Adachi, R., and Südhof, T.C. (2006a). Synaptotagmin-2 is essential for survival and contributes to Ca^{2+} triggering of neurotransmitter release in central and neuromuscular synapses. J. Neurosci. *26*, 13493-13504.

Pang, Z.P., and Südhof, T.C. (2010). Cell biology of Ca^{2+}-triggered exocytosis. Curr. Opin. Cell. Biol. *22*, 496-505.

Pang, Z.P., Sun, J.Y., Rizo, J., Maximov, A., and Südhof, T.C. (2006b). Genetic analysis of synaptotagmin 2 in spontaneous and Ca^{2+}-triggered neurotransmitter release. EMBO J. *25*, 2039-2050.

Pang, Z.P., Xu, W., Cao, P., and Südhof, T.C. (2010). Calmodulin suppresses synaptotagmin-2 transcription in cortical neurons. J. Biol. Chem. *285*, 33930-33939.

Rodriguez-Contreras, A., van Hoeve, J.S., Habets, R.L., Locher, H., and Borst, J.G. (2008). Dynamic development of the calyx of Held synapse. Proc. Natl. Acad. Sci. USA *105*, 5603-5608.

Sabatini, B.L., and Regehr, W.G. (1996). Timing of neurotransmission at fast synapses in the mammalian brain. Nature *384*, 170-172.

Sakaba, T., and Neher, E. (2001). Calmodulin mediates rapid recruitment of fast-releasing synaptic vesicles at a calyx-type synapse. Neuron *32*, 1119-1131.

Schneggenburger, R., and Neher, E. (2000). Intracellular calcium dependence of transmitter release rates at a fast central synapse. Nature *406*, 889-893.

Schneggenburger, R., and Rosenmund, C. (2015). Molecular mechanisms governing Ca^{2+} regulation of evoked and spontaneous release. Nat. Neurosci. *18*, 935-941.

Schonn, J.S., Maximov, A., Lao, Y., Südhof, T.C., and Sorensen, J.B. (2008). Synaptotagmin-1 and -7 are functionally overlapping Ca^{2+} sensors for exocytosis in adrenal chromaffin cells. Proc. Natl. Acad. Sci. USA *105*, 3998-4003.

Skarnes, W.C., Rosen, B., West, A.P., Koutsourakis, M., Bushell, W., Iyer, V., Mujica, A.O., Thomas, M., Harrow, J., Cox, T., *et al.* (2011). A conditional knockout resource for the genome-wide study of mouse gene function. Nature *474*, 337-342.

Sommeijer, J.P., and Levelt, C.N. (2012). Synaptotagmin-2 is a reliable marker for parvalbumin positive inhibitory boutons in the mouse visual cortex. PloS One *7*, e35323.

Sorensen, J.B., Fernandez-Chacon, R., Südhof, T.C., and Neher, E. (2003). Examining synaptotagmin 1 function in dense core vesicle exocytosis under direct control of Ca^{2+}. J. Gen. Physiol. *122*, 265-276.

Südhof, T.C. (2013). Neurotransmitter release: the last millisecond in the life of a synaptic vesicle. Neuron *80*, 675-690.

Sun, J., Pang, Z.P., Qin, D., Fahim, A.T., Adachi, R., and Südhof, T.C. (2007). A dual-Ca^{2+}-sensor model for neurotransmitter release in a central synapse. Nature *450*, 676-682.

Taschenberger, H., Leão, R.M., Rowland, K.C., Spirou, G.A., and von Gersdorff, H. (2002). Optimizing synaptic architecture and efficiency for high-frequency transmission. Neuron *36*, 1127-1143.

Thomas, P., Wong, J.G., and Almers, W. (1993). Millisecond studies of secretion in single rat pituitary cells stimulated by flash photolysis of caged Ca^{2+}. EMBO J. *12*, 303-306.

Ullrich, B., Li, C., Zhang, J.Z., McMahon, H., Anderson, R.G.W., Geppert, M., and Südhof, T.C. (1994). Functional properties of multiple synaptotagmins in brain. Neuron *13*, 1281-1291.

Voets, T., Moser, T., Lund, P.-E., Chow, R.H., Geppert, M., Südhof, T.C., and Neher, E. (2001). Intracellular calcium dependence of large dense-core vesicle exocytosis in the absence of synaptotagmin I. Proc. Natl. Acad. Sci. USA *98*, 11680-11685.

Voiculescu, O., Charnay, P., and Schneider-Maunoury, S. (2000). Expression pattern of a Krox-20/Cre knock-in allele in the developing hindbrain, bones, and peripheral nervous system. Genesis *26*, 123-126.

Wen, H., Linhoff, M.W., McGinley, M.J., Li, G.L., Corson, G.M., Mandel, G., and Brehm, P. (2010). Distinct roles for two synaptotagmin isoforms in synchronous and asynchronous transmitter release at zebrafish neuromuscular junction. Proc Natl Acad Sci U S A *107*, 13906-13911.

Wölfel, M., Lou, X., and Schneggenburger, R. (2007). A mechanism intrinsic to the vesicle fusion machinery determines fast and slow transmitter release at a large CNS synapse. J. Neurosci. *27*, 3198-3210.

Xiao, L., Han, Y., Runne, H., Murray, H., Kochubey, O., Luthi-Carter, R., and Schneggenburger, R. (2010). Developmental expression of Synaptotagmin isoforms in single calyx of Held-generating neurons. Mol. Cell. Neurosci. *44*, 374-385.

Xiao, L., Michalski, N., Kronander, E., Gjoni, E., Genoud, C., Knott, G., and Schneggenburger, R. (2013). BMP signaling specifies the development of a large and fast CNS synapse. Nat. Neurosci. *16*, 856-864.

Xu, J., Mashimo, T., and Südhof, T.C. (2007). Synaptotagmin-1, -2, and -9: Ca^{2+} sensors for fast release that specify distinct presynaptic properties in subsets of neurons. Neuron *54*, 567-581.

Yang, Y.M., Fedchyshyn, M.J., Grande, G., Aitoubah, J., Tsang, C.W., Xie, H., Ackerley, C.A., Trimble, W.S., and Wang, L.Y. (2010). Septins regulate developmental switching from microdomain to nanodomain coupling of Ca^{2+} influx to neurotransmitter release at a central synapse. Neuron *67*, 100-115.

Yoshihara, M., and Littleton, T. (2002). Synaptotagmin I functions as a Calcium sensor to synchronize neurotransmitter release. Neuron *36*, 897-908.

Young, S.M., Jr., and Neher, E. (2009). Synaptotagmin has an essential function in synaptic vesicle positioning for synchronous release in addition to its role as a calcium sensor. Neuron *63*, 482-496.

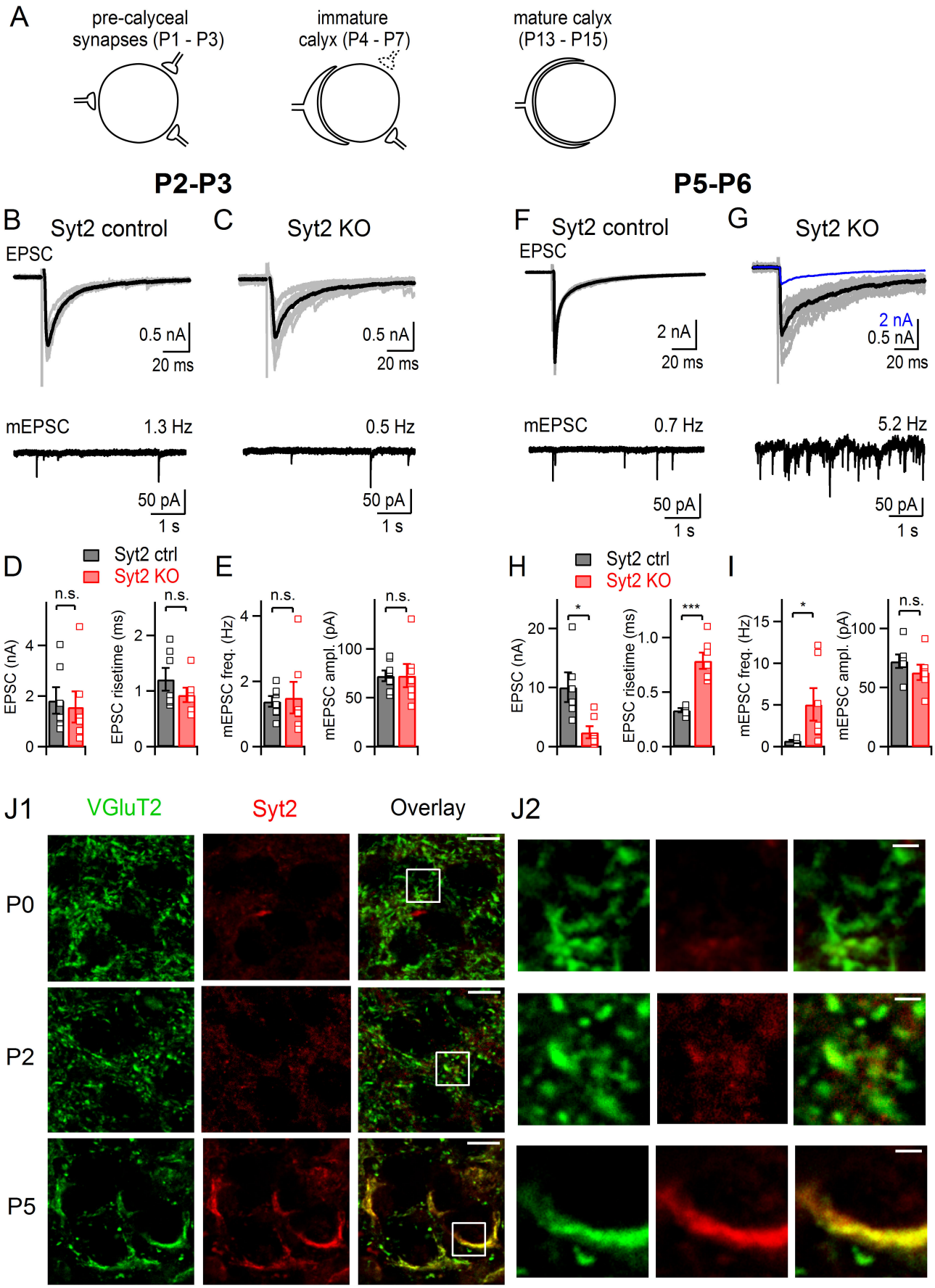
A
pre-calyceal synapses (P1 - P3)
immature calyx (P4 - P7)
mature calyx (P13 - P15)
P2-P3
P5-P6
B Syt2 control
C Syt2 KO
F Syt2 control
G Syt2 KO
EPSC
0.5 nA
20 ms
2 nA
mEPSC
1.3 Hz
0.5 Hz
0.7 Hz
5.2 Hz
50 pA
1 s
D
E
H
I
Syt2 ctrl
Syt2 KO
n.s.
*
***
EPSC (nA)
EPSC risetime (ms)
mEPSC freq. (Hz)
mEPSC ampl. (pA)
J1
VGluT2
Syt2
Overlay
J2
P0
P2
P5

Figure 1

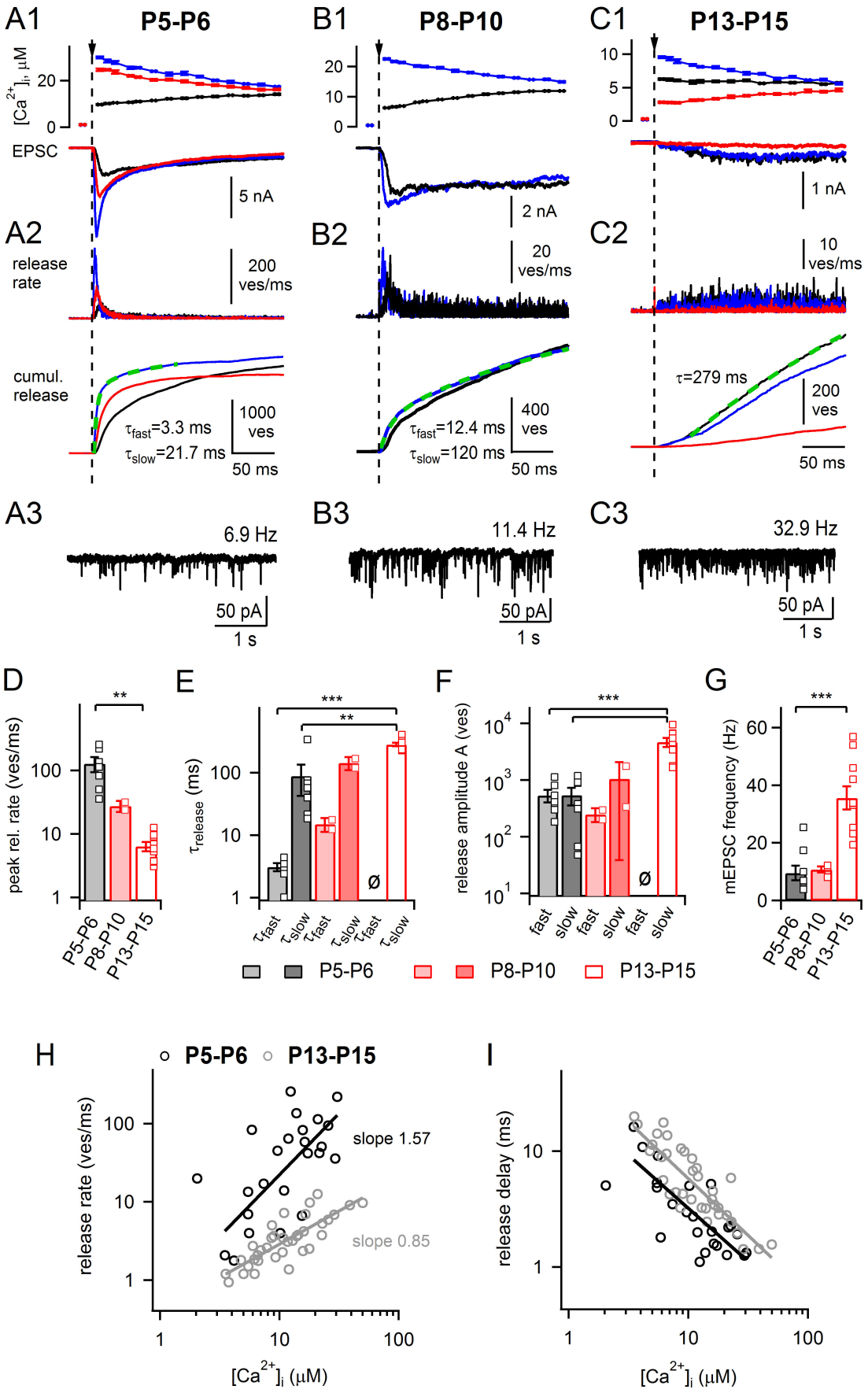
A1
P5-P6
B1
P8-P10
C1
P13-P15
[Ca2+]i, µM
EPSC
5 nA
2 nA
1 nA
A2
B2
C2
release rate
200 ves/ms
20 ves/ms
10 ves/ms
cumul. release
τfast=3.3 ms
τslow=21.7 ms
1000 ves
50 ms
τfast=12.4 ms
τslow=120 ms
400 ves
τ=279 ms
200 ves
A3
B3
C3
6.9 Hz
11.4 Hz
32.9 Hz
50 pA
1 s
D
peak rel. rate (ves/ms)
E
τrelease (ms)
F
release amplitude A (ves)
G
mEPSC frequency (Hz)
P5-P6
P8-P10
P13-P15
H
I
release rate (ves/ms)
slope 1.57
slope 0.85
release delay (ms)
[Ca2+]i (µM)

Figure 2

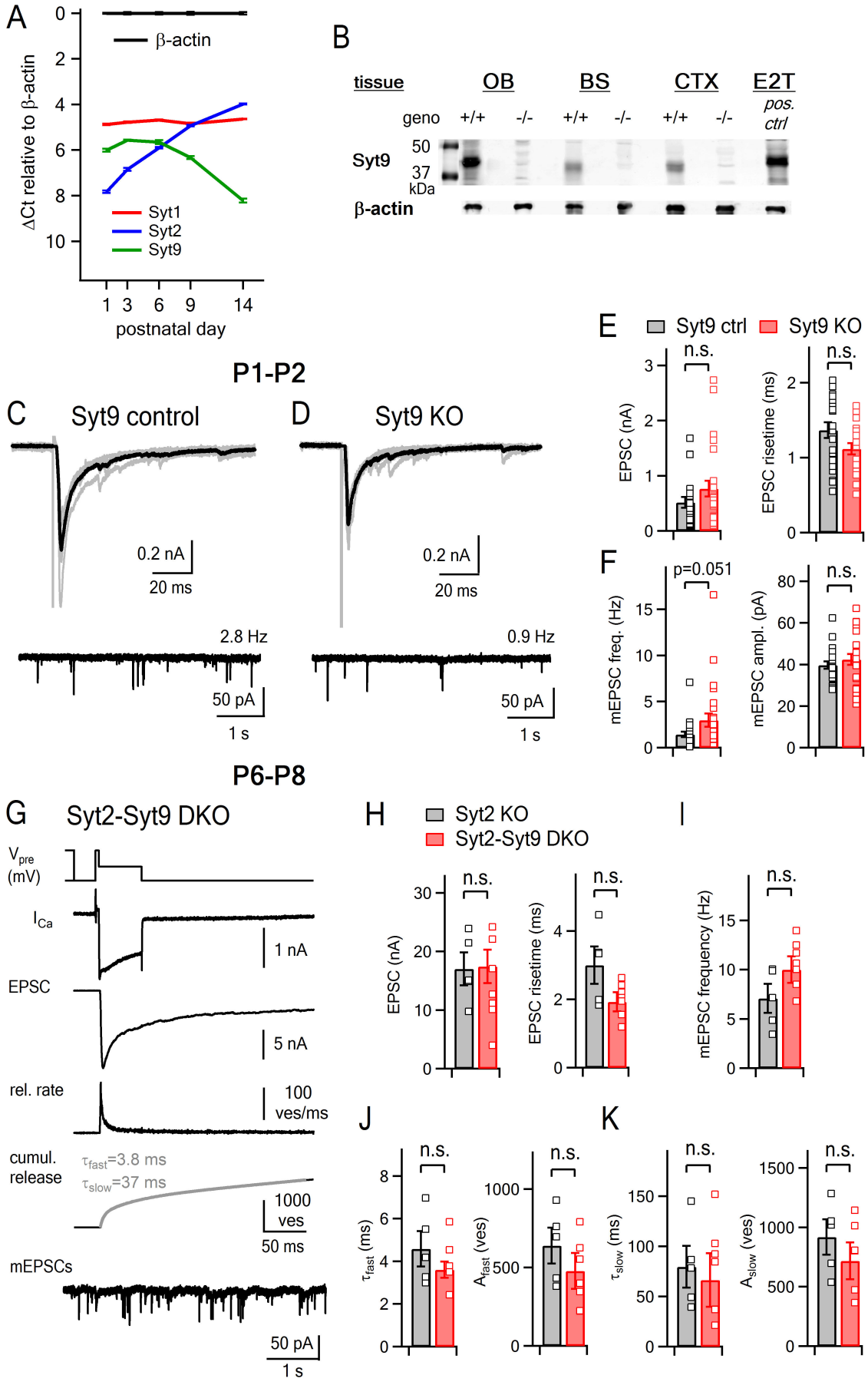
A
β-actin
ΔCt relative to β-actin
Syt1
Syt2
Syt9
postnatal day
B
tissue
OB
BS
CTX
E2T
geno
+/+
-/-
pos. ctrl
Syt9
β-actin
50
37
kDa
P1-P2
C
Syt9 control
D
Syt9 KO
0.2 nA
20 ms
2.8 Hz
0.9 Hz
50 pA
1 s
E
Syt9 ctrl
Syt9 KO
n.s.
EPSC (nA)
EPSC risetime (ms)
F
p=0.051
mEPSC freq. (Hz)
mEPSC ampl. (pA)
P6-P8
G
Syt2-Syt9 DKO
V_pre (mV)
I_Ca
1 nA
EPSC
5 nA
rel. rate
100 ves/ms
cumul. release
τ_fast=3.8 ms
τ_slow=37 ms
1000 ves
50 ms
mEPSCs
50 pA
1 s
H
Syt2 KO
Syt2-Syt9 DKO
I
mEPSC frequency (Hz)
J
τ_fast (ms)
A_fast (ves)
K
τ_slow (ms)
A_slow (ves)

Figure 3

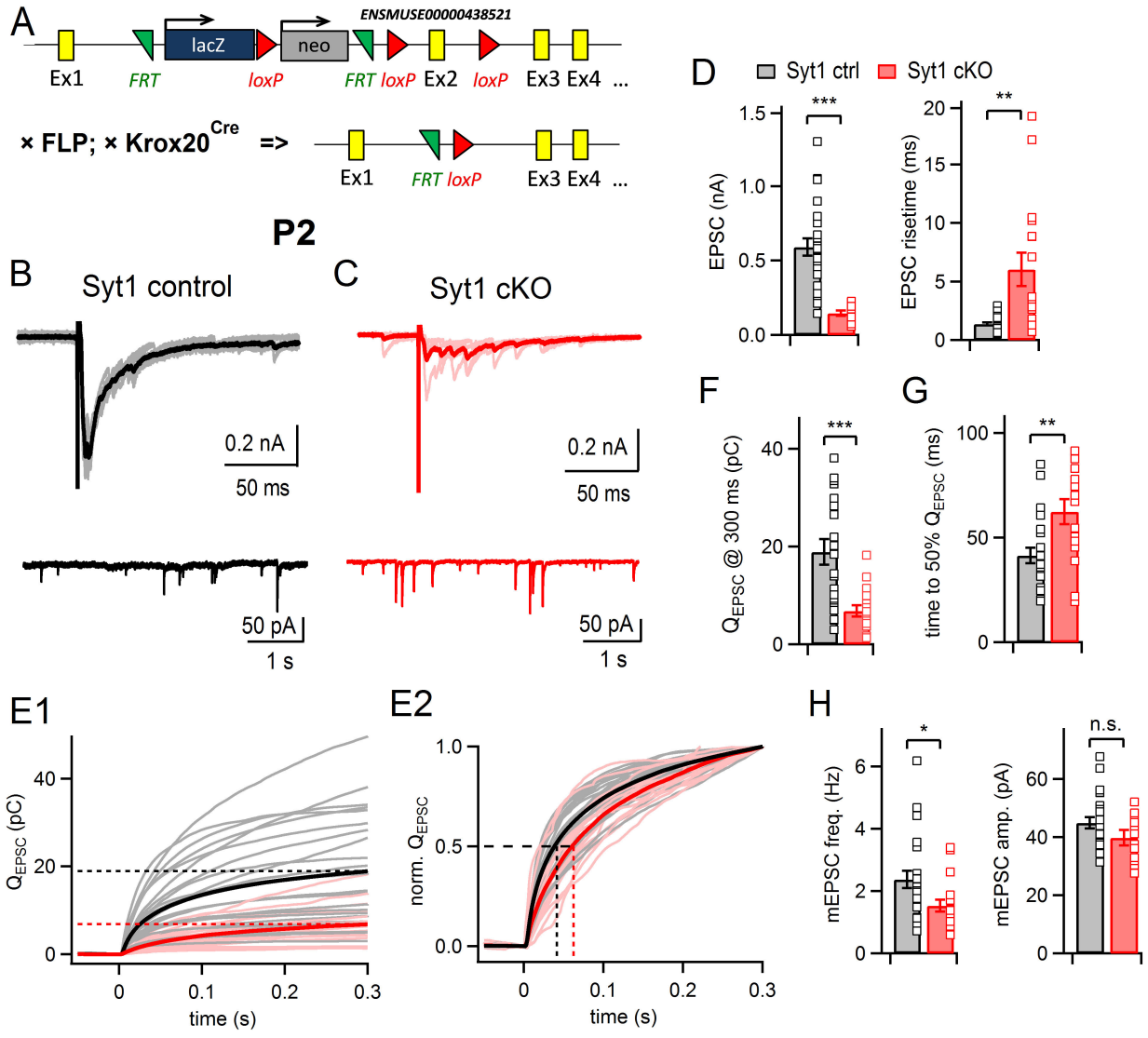
A
ENSMUSE00000438521
lacZ
neo
Ex1
FRT
loxP
FRT loxP
Ex2
loxP
Ex3 Ex4 ...
× FLP; × Krox20Cre =>
Ex1
FRT loxP
Ex3 Ex4 ...
P2
B
Syt1 control
C
Syt1 cKO
0.2 nA
50 ms
50 pA
1 s
D
Syt1 ctrl
Syt1 cKO
EPSC (nA)
EPSC risetime (ms)
F
QEPSC @ 300 ms (pC)
G
time to 50% QEPSC (ms)
E1
QEPSC (pC)
time (s)
E2
norm. QEPSC
time (s)
H
mEPSC freq. (Hz)
mEPSC amp. (pA)
n.s.

Figure 4

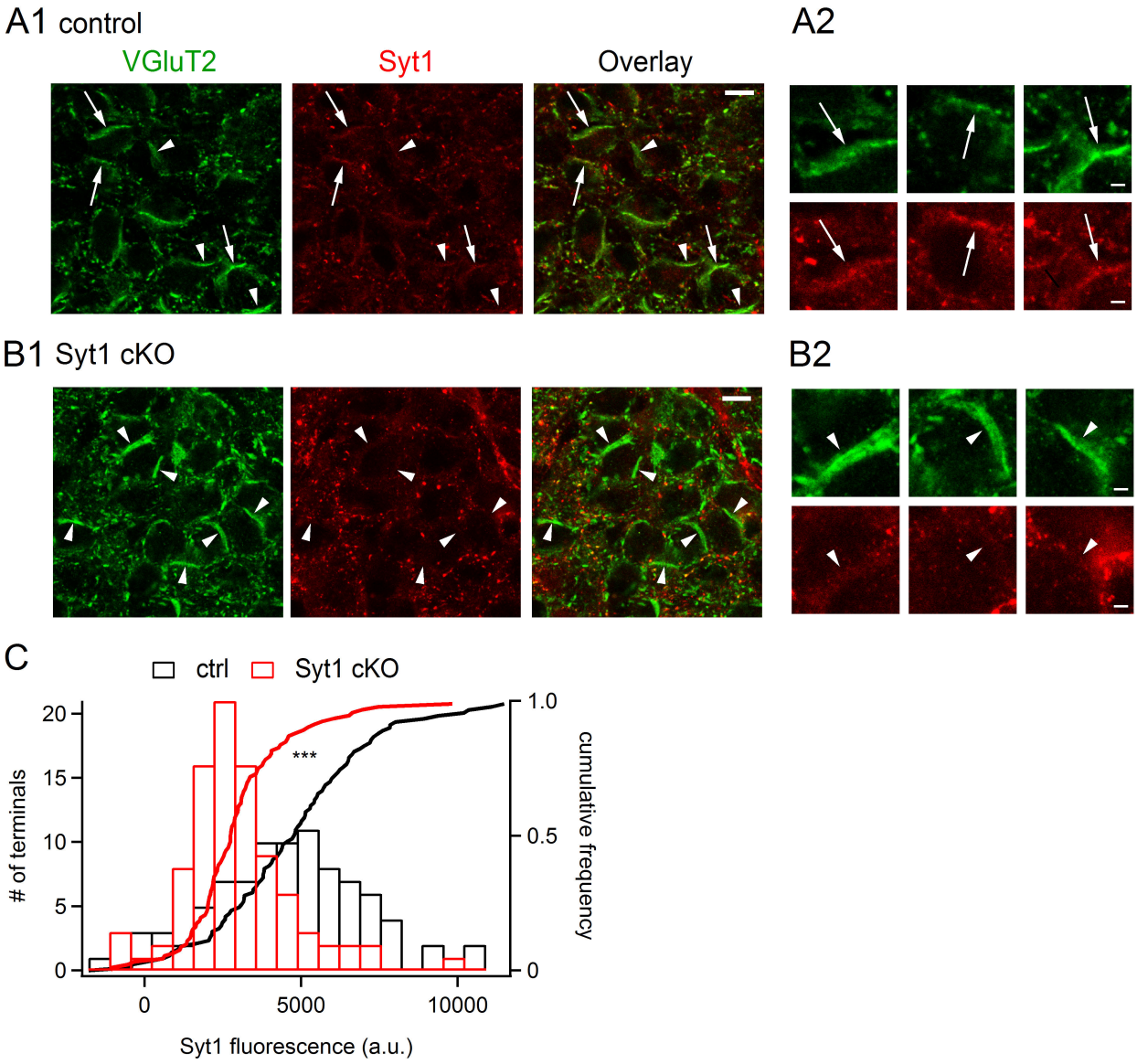
A1 control
VGluT2
Syt1
Overlay
A2
B1 Syt1 cKO
B2
C
ctrl
Syt1 cKO
***
# of terminals
cumulative frequency
Syt1 fluorescence (a.u.)
0
5000
10000
0
5
10
15
20
0
0.5
1.0

Figure 5

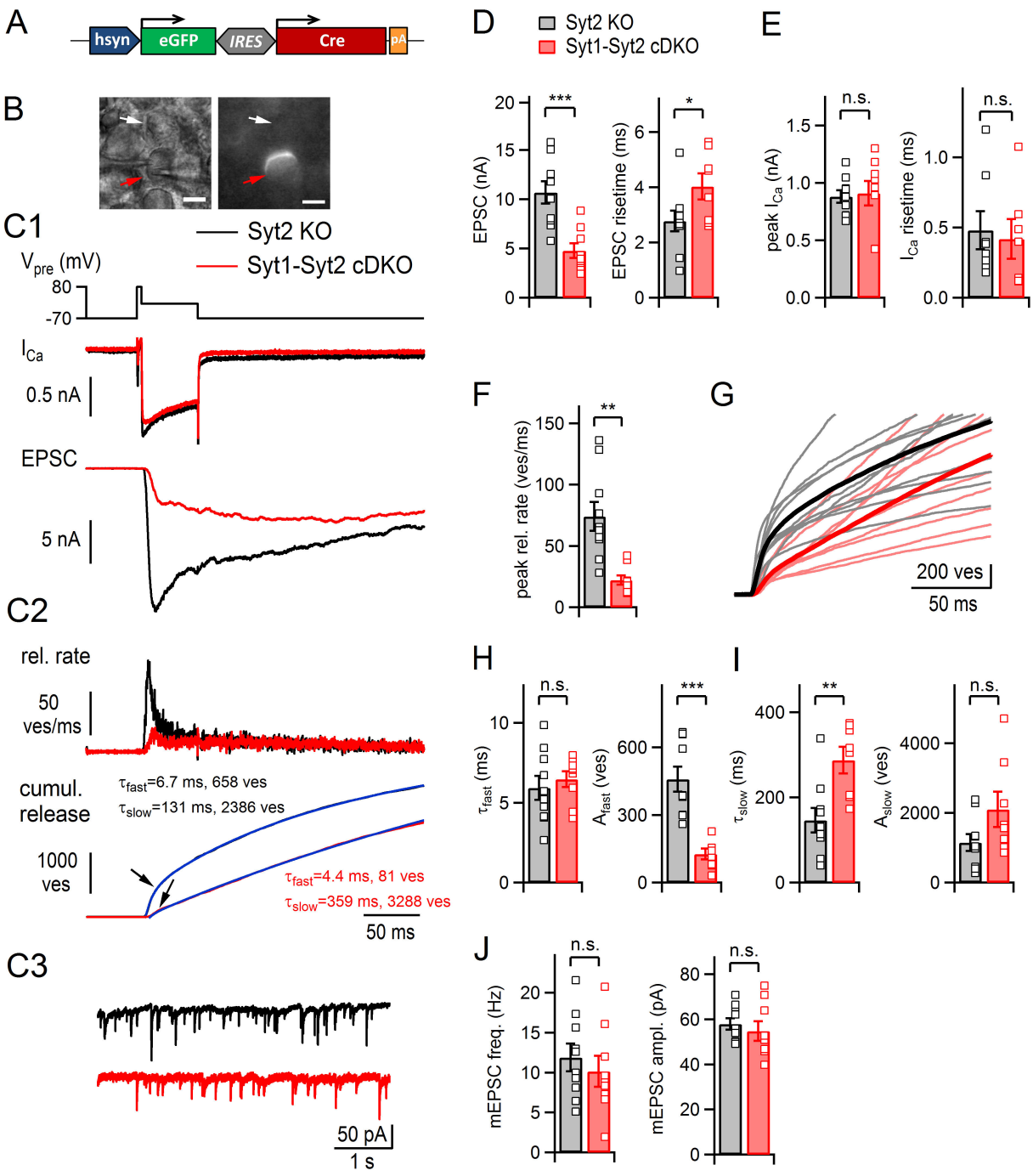
A
hsyn
eGFP
IRES
Cre
pA
B
C1
Syt2 KO
Syt1-Syt2 cDKO
Vpre (mV)
80
-70
ICa
0.5 nA
EPSC
5 nA
C2
rel. rate
50 ves/ms
cumul. release
τfast=6.7 ms, 658 ves
τslow=131 ms, 2386 ves
1000 ves
τfast=4.4 ms, 81 ves
τslow=359 ms, 3288 ves
50 ms
C3
50 pA
1 s
D
Syt2 KO
Syt1-Syt2 cDKO
EPSC (nA)
EPSC risetime (ms)
E
peak ICa (nA)
ICa risetime (ms)
n.s.
F
peak rel. rate (ves/ms)
G
200 ves
50 ms
H
τfast (ms)
Afast (ves)
I
τslow (ms)
Aslow (ves)
J
mEPSC freq. (Hz)
mEPSC ampl. (pA)

Figure 6

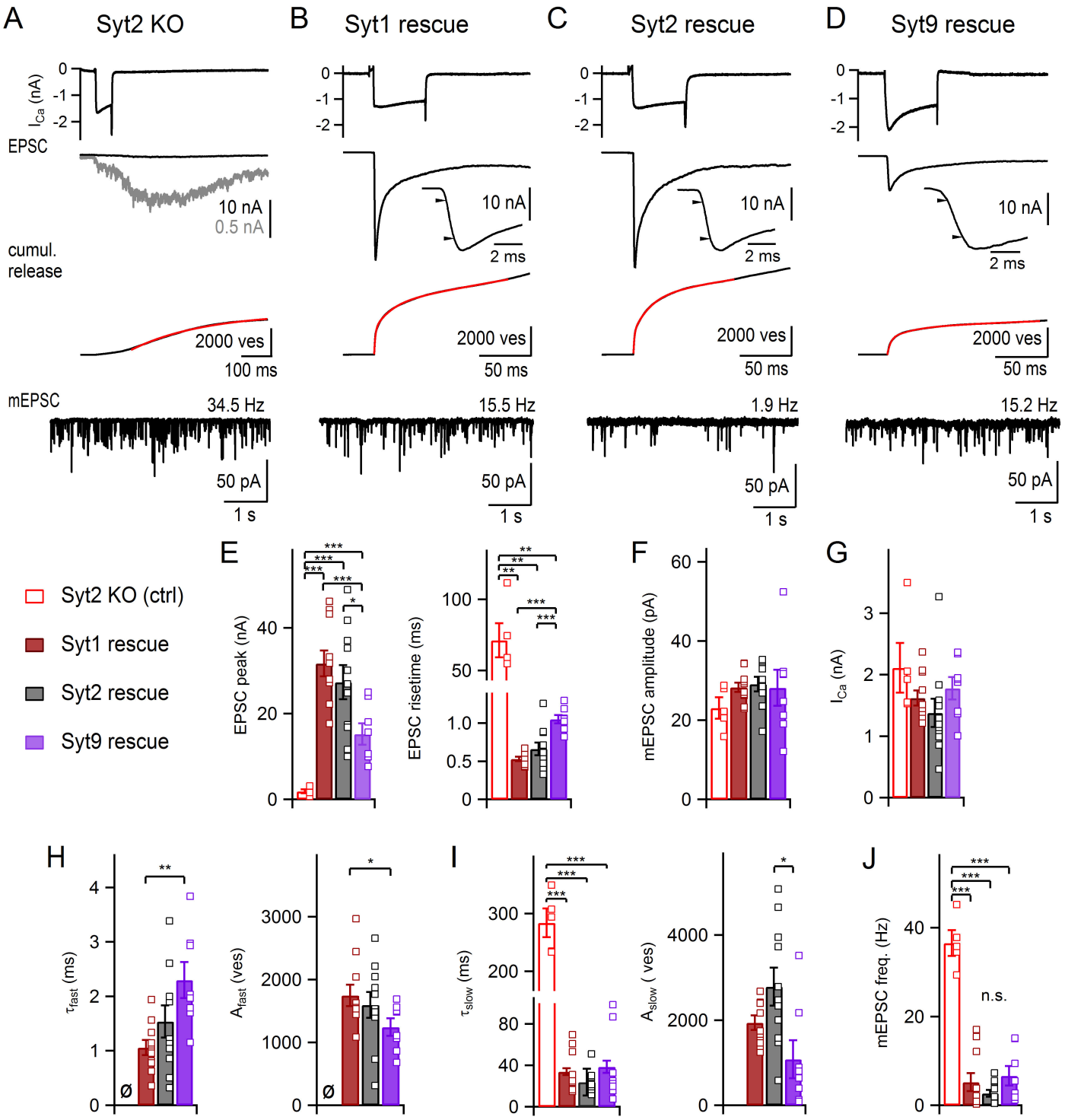
A
Syt2 KO
B
Syt1 rescue
C
Syt2 rescue
D
Syt9 rescue
I_{Ca} (nA)
EPSC
10 nA
0.5 nA
cumul. release
2000 ves
100 ms
50 ms
mEPSC
34.5 Hz
15.5 Hz
1.9 Hz
15.2 Hz
50 pA
1 s
10 nA
2 ms
Syt2 KO (ctrl)
Syt1 rescue
Syt2 rescue
Syt9 rescue
E
EPSC peak (nA)
EPSC risetime (ms)
F
mEPSC amplitude (pA)
G
I_{Ca} (nA)
H
τ_{fast} (ms)
A_{fast} (ves)
I
τ_{slow} (ms)
A_{slow} (ves)
J
mEPSC freq. (Hz)
n.s.

Figure 7

Supplemental Information

A Synaptotagmin isoform switch during the development of an identified CNS synapse

Olexiy Kochubey, Norbert Babai, Ralf Schneggenburger

Inventory:

Supplemental Data

Supplemental Data

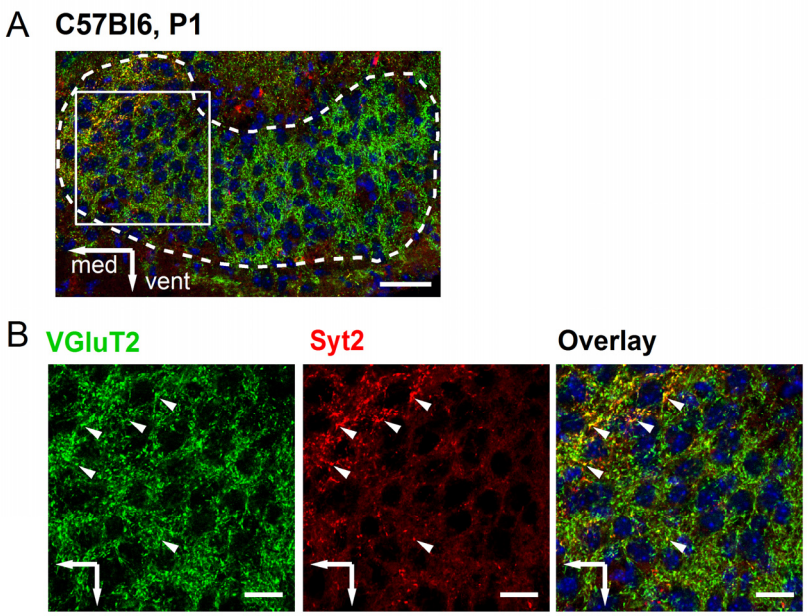

Figure S1. Synaptotagmin2 (Syt2) expression starts early postnatally at the most medial synapses in MNTB. Related to Figure 1.

(**A**) Syt2 expression in glutamatergic synaptic terminals was analyzed in the MNTB nucleus (outlined with the dotted line) of a P1 C57Bl6 mouse using immunostaining against Syt2 and VGluT2 (as in the Results part, Fig. 1). The blue channel represents DAPI stain. Note that the Syt2 signal (red) is absent from the VGluT2-positive puncta (green) virtually throughout the whole MNTB, except a small medial region where co-localization of Syt2 and VGluT2 puncta results in overlay signal (yellow).

(**B**) Higher magnification image of the area marked with the white square in (A). Arrowheads highlight VGlut2-positive synaptic terminals which also express Syt2. Thus, most pre-calyceal excitatory synapses in the MNTB at P1 do not express Syt2, except the most medial synapses. Scale bars 50 and 20 µm in (A) and (B), respectively.

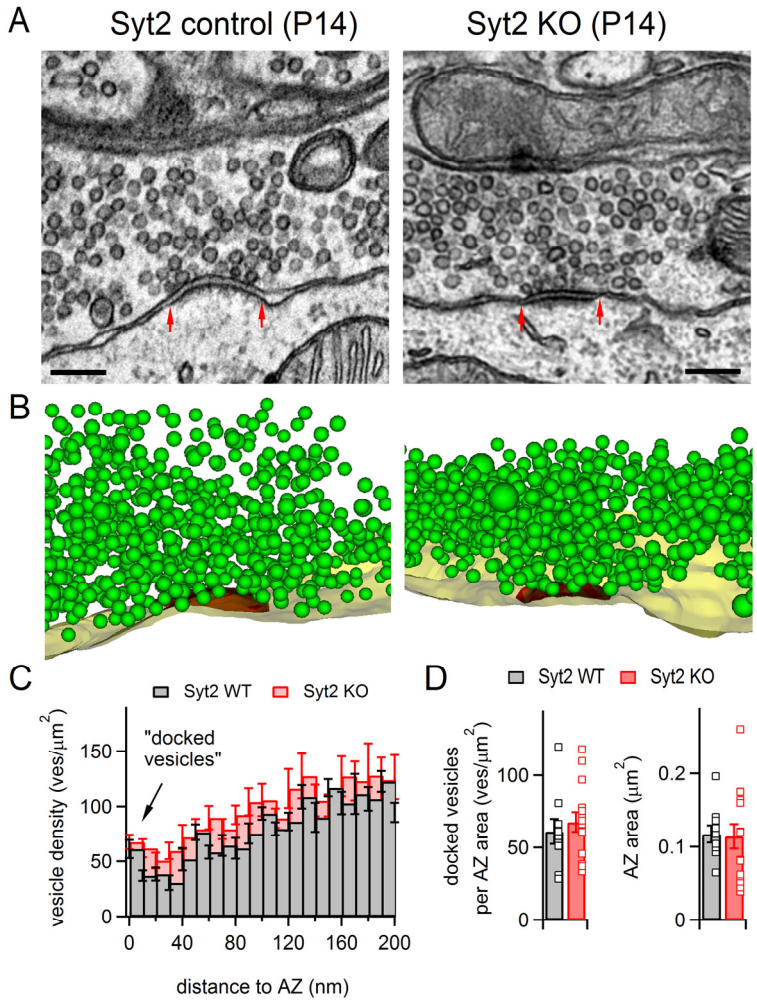

Figure S2. Ultrastructural analysis of active zones shows no docking defect in mature calyx of Held synapses from Syt2 KO mice. Related to Figure 2.

In order to study the possible effects of Syt2 deletion on vesicle docking, we performed transmission electron microscopy (tEM), and reconstructed single active zones in the calyces of a Syt2 KO versus a $Syt2^{+/+}$ mouse at P14 (see Supplemental Experimental Procedures).

(**A**) Representative tEM images of serial sections through the middle of active zones of the calyx of Held synaptic terminals from a Syt2 control mouse ($Syt2^{+/+}$, *left*) and from a Syt2 KO mouse ($Syt2^{-/-}$; *right*). Red arrows indicate the AZ borders. Scale bar, 200 nm.

(**B**) 3D-rendering results of the reconstructed AZs, corresponding to the example EM images shown in (A). The presynaptic membrane (yellow), active zones (red) and synaptic vesicles (green) were incorporated.

(**C**) Average distributions of the vesicle densities per AZ area as a function of membrane-to-membrane distance between synaptic vesicles and the active zones, for Syt2 KO (red; n = 15 AZs from N=3 calyces) and control mouse (black; n=10 AZs from N=5 calyces). Histogram bin size was 10 nm; we define vesicles with a distance of 10 nm or less to the presynaptic membrane as "docked" vesicles (first bin). Note that the overall vesicle density seems higher at Syt2 KO active zones. To test this difference we compared the density of vesicles within shells of 200 and 500 nm radius from the active zone, but it was not statistically significant (p = 0.211 and p = 0.396, respectively).

(**D**) The density of docked vesicles (the first bin of the histogram in C) was not significantly different between the two groups (61 ± 9 in Syt2 control; n = 10 active zones versus 68 ± 7 ves/µm^2 in Syt2 KO; n = 15 active zones). The active zone (AZ) area was also not changed in the Syt2 KO (0.114 ± 0.017 µm^2, n=15) compared to the Syt2 control (0.117 ± 0.012 µm^2, n=10).

These results suggest that the strong slowing of transmitter release observed in Syt2 KO mice at P13 - P15 (see Figures 2, 7), is not caused by a deficit of vesicle docking at the active zone.

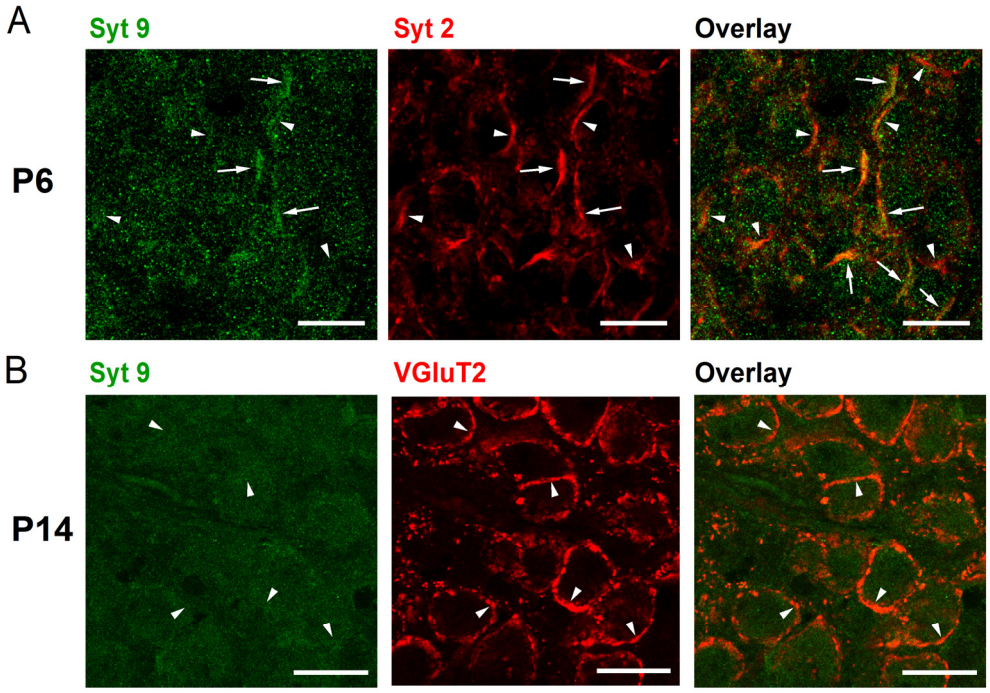

Figure S3. Syt9 is weakly expressed at immature calyces of Held (P6) but absent from mature calyces (P14). Related to Figure 3.

In order to study the developmental expression profile of Syt9 protein at the calyx of Held synapse, we performed immunohistochemistry with an anti-Syt9 antibody (see Supplemental Experimental Procedures) in the MNTB nucleus in mice at P6 and at P14.

(**A**) At P6, some calyces identified by Syt2 IHC (red channel) co-express Syt9 (left panel, green channel; arrows). *Arrows*, examples of calyces with detectable Syt9 staining; *arrowheads,* Syt2-positive calyces without detectable Syt9 signal.

(**B**) At P14, no detectable immunofluorescence signal was observed with the Syt9 antibody; calyces in this example were detected with an anti-VGluT2 antibody (red channel, middle; *arrowheads,* examples for VGluT2 - positive calyces without detectable Syt9 signal). Note that following virus-mediated overexpression of Syt9, the same antibody clearly detected the recombinant Syt9 protein (see Fig. S5B2). We conclude, therefore, that Syt9 is only expressed weakly at some immature calyces, but that it is absent from mature calyces at P14.

Scale bars are 20 µm.

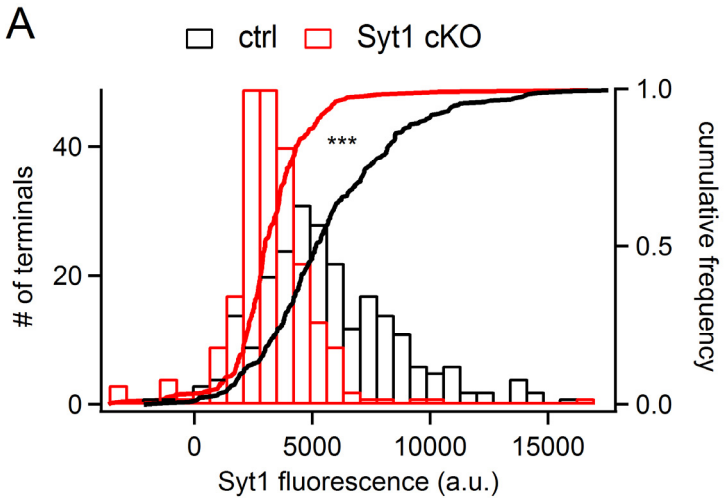

Figure S4. A significant reduction of Syt1 immunoreactivity in immature calyces upon conditional deletion of Syt1 is observed reproducibly. Related to Figure 5.

The histograms and cumulative histograms shows the same analysis as performed for Fig. 5 C, in a second pair of a Syt1 cKO mouse ($Syt1^{\Delta/lox}$, $Krox20^{+/Cre}$ genotype) and its littermate control mouse ($Syt1^{\Delta/lox} \times Krox20^{+/+}$ genotype; both mice at P5). All samples were processed and imaged in parallel, with the same antibody dilutions (Syt1Cl41.1 at 1:150) and the same settings for confocal imaging. We again observed a highly significant reduction of the anti-Syt1 immunofluorescence signal analyzed in the areas of calyces of Held defined by the anti-VGluT2 staining (see Fig. 5A, B; n = 241 and 225 calyx-masks analyzed for the control mouse and the Syt1 cKO mouse, respectively; $p < 1e\text{-}9$, Kolmogorov-Smirnoff test; D-statistic = 0.461).

We therefore conclude that the weak Syt1 immunofluorescence signal present in immature calyces at P5 is a specific signal, since it is significantly reduced in Syt1 cKO mice.

In yet another series of stainings, we used an alternative anti-Syt1 antibody (mAb48 1:100; Developmental Studies Hybridoma Bank, University of Iowa). Note that despite overall similar staining pattern – bright small puncta throughout MNTB that do not co-localize with the calyceal profiles (see also Fig. 5A, B) – we did *not* observe a clear Syt1-specific signal within the calyx terminals with this alternative antibody. We conclude, therefore, that possible differences between antibodies might preclude the detection of low levels of Syt1 expression.

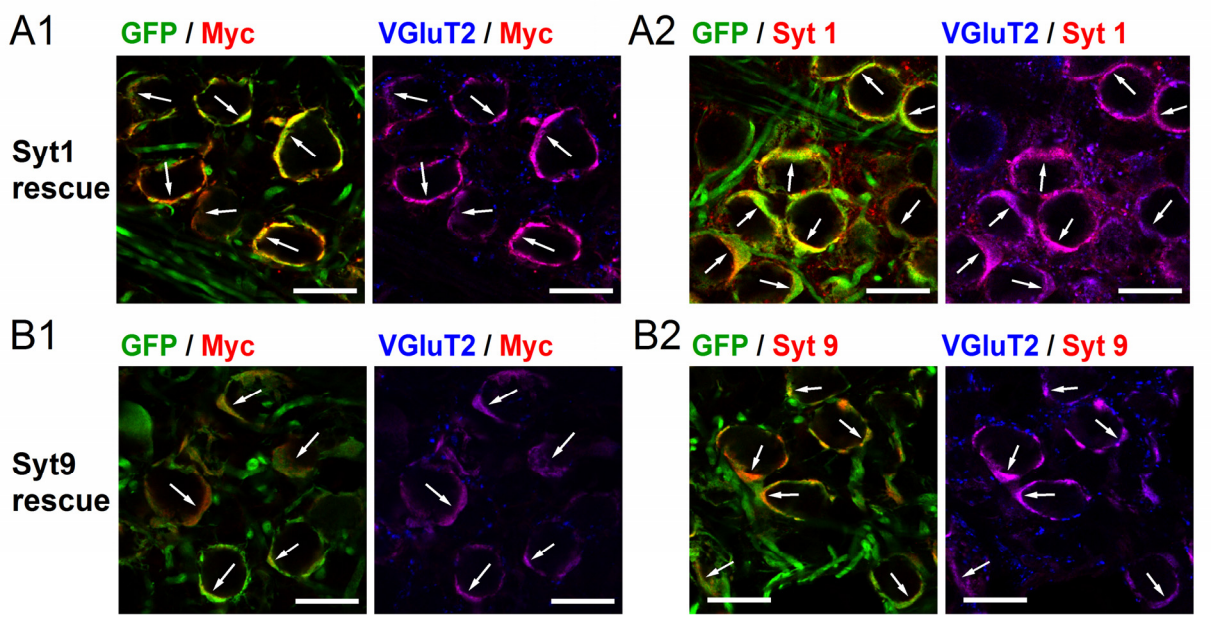

Figure S5. Viral expression of Syt1 and Syt9 rescue constructs leads to targeting of both proteins to calyx of Held nerve terminals. Related to Figure 7.

In order to confirm proper targeting of Syt1 and Syt9 proteins to calyx of Held presynaptic terminals in the rescue experiments (Fig. 7), we injected Syt2 KO mice at P7 with the indicated rescue construct (MycSyt1 or MycSyt9), and then performed immunohistochemistry at P14 (same time interval as for the functional rescue experiments in Fig. 7).

(**A1**) Presynaptic profiles of the calyx of Held synapses visualized by anti-Myc (red channel; Alexa647), anti-GFP (green, Alexa488) and anti-VGluT2 (blue; Alexa 568) in a MycSyt1 rescue experiment. Note that in this field of view, most calyces were transduced (thus, GFP-positive). Transduced calyces also show a bright anti-Myc staining which is limited to the calyces and largely overlaps with anti-VGluT2 staining (right panel, see arrows).

(**A2**) In another section of the MNTB of the same mouse (MycSyt1 rescue), we used an anti-Syt1 antibody (A2, red channel; Alexa647), and again the anti-GFP and anti-VGluT2 antibodies (green and blue channels, respectively). Note the clear expression of the recombinant Syt1 protein detected by the anti-Syt1 antibody, whereas non-infected calyces do not show a detectable Syt1 signal at this age (not shown). Note that this experiment also further validates the specificity of the anti-Syt1 antibody.

(**B1, B2**) Same experiment as in (A1, A2), but now following injection of the Syt9-Myc rescue construct in a Syt2 KO mouse at P7. Note the clear presence of recombinant Syt9 protein in transduced (GFP-positive) calyces of Held, as indicated by the anti-Myc antibody (B1, red channel), and by the anti-Syt9 antibody in another section (B2, red channel). Note that this experiment also validates the anti-Syt9 antibody, which clearly detects recombinant Syt9 protein after virus-mediated overexpression (B2), but which gives only weak or no signals in wild - type calyces of Held at P6 and P14, respectively (see Figure S3). Finally, note that the anti-Myc signal is, on a qualitative level, weaker for the MycSyt9 construct than for the MycSyt1 construct (compare red channels in A1 versus A2). It is possible, therefore, that rescue with the Syt9 construct leads to lower protein levels in calyx of Held nerve terminals than rescue with the Syt1 construct.

Scale bars are 20 µm.

Supplemental Experimental Procedures

Supplemental Experimental Procedures for Synaptotagmin mouse lines.

Due to postnatal lethality of the homozygous Syt2 KO mice at ~ 3 weeks of age (Pang et al., 2006; RRID:MGI_3696550), Syt2 KO mice (mice with $Syt2^{-/-}$ genotype in all breedings) were sacrificed at P16 at latest, complying with the Veterinary office's guidelines (see Experimental Procedures).

The Syt9 line (gene accession NM_016908, Xu et al., 2007) was purchased from Jackson Labs as a conditional mutant line (B6;129-$Syt5^{tm2Sud}$; RRID:MGI_3715455). However, this Syt9 line was a conventional KO, since in the previous breeding history a cross with a ubiquitous Cre carrier took place. We confirmed constitutive deletion of the Syt9 exon 2 and the presence of N-terminal EmGFP transgene in-frame with the remaining exon 1 by sequencing the PCR fragment amplified from the homozygous mutant genomic DNA using the primers 5'-CCAACGAGAAGCGCGATCACATGG and 5'-GTTGAGATGTAATGTATACCTATGC, targeting respectively the 3'-end of EmGFP cassette and genomic sequence downstream of the exon 2 of Syt9 (Xu et al., 2007). Syt2 - Syt9 DKO mice were obtained by double-heterozygous crossing between Syt2 and Syt9 lines.

The Syt1lox mouse line $Syt1^{tm1a(EUCOMM)Wtsi}$ (purchased from EMMA, Monterotondo, Italy; EM06829; RRID:MGI_5450372) was acquired as frozen sperm stock and re-derived in female mice of C57Bl6 background carrying a constitutively expressing FLP gene in order to remove the Frt-flanked lacZ/neo insert (Fig. 4A; homozygous animals for this insertion are not viable probably due to a disrupted gene function; EMMA). Re-derivation was done using a standard in-vitro fertilization procedure at the SPF-grade transgenesis facility of EPFL. FLP recombinase gene was then eliminated in the following breeding history. The resulting $Syt1^{lox/+}$ offspring animals were crossed with the hemizygous $Krox20^{Cre}$ mice (Voiculescu et al., 2000; Han et al., 2011) to obtain mice with brainstem-specific deletion of Syt1 gene (Fig. 4). Due to germline recombination in the Krox20Cre line (Voiculescu et al., 2000), one of each floxed Syt1 alleles was deleted in these mice, as indicated by the $^{\Delta}$ symbol. Attempts to cross the conventional Syt2 KO mice with the $Syt1^{floxed}$ and $Krox20^{Cre}$ mice to produce brainstem-specific conditional Syt1 KO in the absence of Syt2 (Syt1 – Syt2 cDKO) did not result in viable offsprings. Thus, in a cohort of 120 genotyped pups with Mendelian expectation of 6 cDKO animals, only 2 were recovered which perished immediately after birth. This perinatal lethality might be caused by Krox20Cre - mediated recombination of the floxed Syt1 alleles in brainstem areas relevant for breathing regulation (Chatonnet et al., 2007), which would then lack both Syt isoforms. To restrict conditional Syt1 deletion to the calyx synapses in Syt2 KO background, we used a virus-mediated Cre-expression approach (see below).

Syt1 genotyping was done using the standard PCR technique with the common forward primer 5'-GATTCATGATGTCACTGAATCCTATGC, and the reverse primers 5'- TCATTTACACGTCGCTTGCC or 5'-TCGTGGTATCGTTATGCGCC for the wildtype or mutant reactions, detecting fragments of intact intronic sequence upstream of exon 2, or the exogenous cassette introduced by the targeting vector, respectively.

Supplemental Experimental Procedures for viral vectors and stereotaxic surgery

Second generation adenovirus vectors were prepared and stereotactically injected as described previously (Kochubey and Schneggenburger, 2011; Genç et al., 2014). Briefly, an eGFP expression cassette, or an eGFP-ires-CreT expression cassette was subcloned downstream of the human synapsin1 (Hsyn1) promoter in the pDC511 adenoviral shuttle vector (Microbix Biosystems, Ontario, Canada) which was co-transfected into E2T packaging cells together with the custom-modified 2a-deleted pBHGfrtΔ1,3FLP backbone plasmid (Microbix Biosystems; see also Zhou and Beaudet, 2000; Young and Neher, 2009). For the rescue experiments (Fig. 7), Syt1 or MycSyt1, MycSyt2, or MycSyt9 sequences were subcloned downstream of the Hsyn1 promoter in pDC511 vector which was then used with a different pBHGfrtΔ1,3FLP backbone carrying another Hsyn1 driven cassette expressing eGFP (a kind gift of Dr. Sam Young). Propagation, plaque purification and concentration of the adenoviral particles was done as previously described (Kochubey and Schneggenburger, 2011) using Adenopack 100 RT kit (Sartorius, Aubagne, France), resulting in ~750 µl viral stock in the injection-ready storage buffer (in mM: 250 sucrose, 10 HEPES, 1 $MgCl_2$, pH 7.4) with the final titer of $1\text{-}2 \cdot 10^{12}$ ml^{-1} (OD_{260}).

Stereotactic injections into the VCN of P0 - P1 $Syt1^{lox/lox}$/Syt2KO mouse pups (Fig. 6) was done on a model 900 stereotactic instrument (Kopf Instruments, Tujunga, CA) under continuous 1-1.5% isoflurane anaesthesia. Lambda point, notable through the skin, was aligned horizontally with a midline point 3.7 mm anterior from

lambda, and the skin was co-punctured together with the skull bone at two points located 0.3 and 0.9 mm posterior, both 1.57 mm lateral from lambda. A 35G stainless steel needle (Coopers Needle Works, Birmingham, UK) was lowered through the two punctures to deliver 0.25 µl virus at each of the three injection sites (with the lower site at 4.2 mm from the surface, spaced vertically 0.15 mm apart). A slow injection rate (80 nl/min) was achieved using a Model 11 syringe pump (Harvard Apparatus, Holliston, MA) operating with a 10 µl syringe (Hamilton, Bonaduz, Switzerland). After full recovery from anaesthesia (~30 - 45 min) the pups were put back to the mother. Injections into VCN of P6 pups for the rescue experiments (Fig. 7) was done as described previously (Kochubey and Schneggenburger, 2011).

Supplemental Experimental Procedures for Slice electrophysiology and Ca^{2+} uncaging

Two-hundred µm thick coronal slices containing MNTB were cut using a Leica VT 1000S slicer (Leica Microsystems, Wetzlar, Germany) and kept before use in a storage chamber with a bicarbonate-buffered incubation/recording solution at 37°C (in mM: 125 NaCl, 25 $NaHCO_3$, 2.5 KCl, 1.25 NaH_2PO_4, 25 glucose, 2 $CaCl_2$; 1 $MgCl_2$, 0.4 ascorbic acid, 3 myo-inositol and 2 Na-pyruvate; all from Sigma, Buchs, Switzerland), bubbled with 95% O_2/5% CO_2 (pH 7.4). Recordings were done at room temperature (22 - 24°C) using an EPC-10/2 patch-clamp amplifier (HEKA Elektronik, Lambrecht/Pfalz, Germany) and an upright BX-51 microscope (Olympus, Tokyo, Japan) equipped with a 60x/0.9NA immersion objective (Olympus). A Sensicam QE CCD camera (PCO, Kelheim, Germany) under control of TILLVision software (FEI München, Gräfelfing, Germany) was used to visualize cells with Dodt IR gradient contrast. The same camera was also used for Ca^{2+} imaging during Ca^{2+} uncaging experiments (see below). For afferent fiber stimulation, a custom platinum-iridium bipolar electrode was placed close to the medial border of MNTB, and short (0.2 ms) pulses of 0 - 40 V amplitude were delivered from an isolated stimulator (A-M Systems, model 2100, Carlsborg, WA, USA). During these experiments, 10 µM bicuculline methochloride, 100 µM cyclothiozide (CTZ), 50 µM D-(-)-2-Amino-5-phosphonopentanoic acid (D-APV; all from BIOTREND, Wangen, Switzerland), and 2 µM strychnine (Sigma) were added to the recording solution. The cells in the medial extremity of MNTB were excluded from the fiber stimulation recordings in P2 - P3 mice (Figs. 1, 3, 4) to avoid possible bias due to the early onset of Syt2 expression in that region (see Fig. S1). For pre- and postsynaptic recordings, the bath solution was further supplemented with 1 µM tetrodotoxin (Biotrend) and 10 mM tetraethylammonium (TEA) chloride (Sigma). In all Syt1 and Syt2 rescue experiments, and for some (n=3) Syt9 rescue recordings (Fig. 7), 2 mM γ-D-glutamylglycine (γ-DGG; BIOTREND) was added. To allow direct comparison between datasets within Fig. 7, mEPSC and EPSC amplitudes recorded without γ-DGG were scaled with a factor of 0.5.

The series resistance (R_s) during pre- and postsynaptic recordings was in the range of 8 - 25 MOhm and 4 - 10 MOhm, respectively, and was compensated by 50 - 80% by the patch-clamp amplifier. EPSCs were recorded at the lowest possible gain (0.5 mV/pA) for the intermediate feedback resistor of the EPC10 amplifier, which allowed us to record currents of up to - 20 nA amplitude. To avoid amplifier saturation when EPSCs were > 20 nA at the standard holding potential (V_h) of -70 mV, V_h was set to either -50, -40 or -30 mV in some recordings, most notably in some rescue experiments (Fig. 7). During off-line analysis, EPSCs were first corrected for the remaining R_s error as described in (Meyer et al., 2001). When EPSCs were recorded at a lower V_h than - 70 mV, they were then additionally re-scaled to their expected value at V_h=-70 mV, assuming a reversal potential for EPSCs of 0 mV. These procedures often resulted in EPSC with nominal amplitudes of 20 - 40 nA at a V_h of - 70 mV (Fig. 7E). Two cells with EPSC amplitudes ~ 60 nA (one expressing Syt1 and the other - MycSyt1; Fig. 7) were excluded from the analysis as outliers. For Syt1 rescue, we initially used a non-Myc tagged rescue construct (n = 6 cells), and later a Myc-tagged Syt1 construct (n = 5 cells). However, the datasets were not statistically different ($p > 0.05$), and were therefore pooled together in Fig. 7.

The patch pipette solution contained (in mM): 140 Cs-gluconate, 20 TEA, 10 HEPES, 5 Na_2-phosphocreatine, 4 MgATP, 0.3 Na_2GTP, pH 7.2 adjusted with CsOH, and was supplemented with 5 or 0.1 mM Cs-EGTA for post- or presynaptic recordings, respectively.

For Ca^{2+}-uncaging and imaging (Fig. 2), the presynaptic solution contained (in mM): 140 Cs-gluconate, 20 TEA, 20 HEPES, 5 Na_2ATP, 0.3 Na_2GTP, pH 7.2 adjusted with CsOH, supplemented with 2 DM-Nitrophen (Merck Chemicals, Nottingham, UK), 1.75 $CaCl_2$, 0.5 $MgCl_2$ and 100 µM fura-2FF (TefLabs, Austin, TX, USA). A xenon arc flash lamp (SP-20; Rapp OptoElectronic, Hamburg, Germany) and a set of neutral density filters was used to generate 0.4 - 0.5 ms UV flashes of different intensities to induce DMN photolysis. A Polychrome V monochromator (FEI München, Gräfelfing, Germany) was used for ratiometric imaging of post-flash $[Ca^{2+}]_i$ with alternating 350 and 380 nm UV excitation light pulses of 5 ms; the resulting fura-2FF fluorescence was imaged with a Sensicam QE CCD camera (PCO, Kelheim, Germany; 8x8 pixel binning). Fura-2FF was calibrated for quantitative ratiometric Ca^{2+} imaging as described (Kochubey and Schneggenburger, 2015).

Analysis of electrophysiological data was done in IgorPro 6.3 (Wavemetrics, Lake Oswego, OR) using custom routines. A template-matching algorithm (Clements and Bekkers, 1997) was implemented to detect mEPSCs. Transmitter release rates were calculated by deconvolving the quantal EPSC waveform from the measured EPSCs, using analysis routines first described by Neher and Sakaba (2001). The average mEPSC waveform analyzed for each recording was used as a quantal waveform template for the deconvolution. Transmitter release rates were corrected for the estimated spill-over glutamate current; the parameters for setting the spill-over current were constrained by initially giving "template protocols" (Neher and Sakaba, 2001). In older Syt2 KO synapses which showed almost no synchronous release this approach was not possible, and the spill-over current parameters were set to similar values as those observed in control synapses of the corresponding age. The time-course of cumulative release was fitted by the following functions: exponential, exponential plus line, double exponential, double exponential plus line, and triple exponential, and a Bayesian information criterion was used to determine the optimal fit function, which was a double exponential plus line in most cases.

Supplemental Experimental Procedures for qPCR, immunohistochemistry, and Western blot

For qPCR analysis of Syt1, Syt2 and Syt9 mRNA expression (Fig. 3A), the VCN brain samples were pooled from two C57Bl6 mice at every age (P1, P3, P6, P9 and P14), and the total RNA was extracted under RNase-free conditions using a RNeasy Plus Micro kit (Qiagen, Germantown, MD). Equal amounts (270 ng) of each RNA sample was used to produce cDNA libraries using a High-Capacity Reverse Transcription kit (Life Technologies, Zug, Switzerland). The qPCR reactions were run in 10 µl total volume with the input amount of cDNA corresponding to 1 ng total RNA, using TaqMan assays for Syt1 (Mm00436858_m1), Syt2 (Mm00436864_m1), Syt9 (Mm00444196_m1) and β-actin (Mm01205647_g1) in an ABI 7900HT real-time PCR system (Life Technologies). The reactions were done in triplicates for each sample and probe, and the analysis (average CT values and normalization to β-actin signal) was performed using a custom macro in IgorPro.

Immunohistochemistry (Figs. 1, 5, S1, S3- S5) was done as follows. A given mouse was deeply anaesthetised with pentobarbital injection, and transcardially perfused with 4% paraformaldehyde in phosphate buffered saline. After post-fixation (24 hours at 4°C), the brain was dehydrated in 30% sucrose solution, and the brainstem tissue was cut frozen at MNTB level into 40 µm coronal sections using a sliding microtome Hyrax S30 (Carl Zeiss, Oberkochen, Germany). Free-floating sections were permeabilized, blocked and incubated overnight at 4°C with primary antibodies as indicated: mouse anti-Syt1 (1:150; Synaptic Systems 105011, Göttingen, Germany; RRID: RRID:AB_887832), mouse anti-Syt2 (1:750; znp-1; ZIRC, Eugene, OR; RRID:AB_10013783), rabbit anti-Syt5/9 (1:250 to 1:500; Synaptic Systems 105053; RRID:AB_2199639), guinea pig anti-VGluT2 (1:500; Synaptic Systems 135404; RRID:AB_887884), chicken anti-GFP (1:1000; Abcam 13970, Cambridge, UK; RRID:AB_300798), mouse anti-Myc 9B11 (1:500; Cell Signaling Technology #2276, Leiden, Netherlands; RRID:AB_331783). The corresponding secondary antibodies from the following list (all from Life Technologies, Carlsbad, CA) were incubated with the sections for 1h at RT at 1:200 dilution: goat anti-rabbit Alexa488 (A11034; RRID:AB_10562715), goat anti-chicken Alexa488 (A11039; RRID:AB_10563770), goat anti-guinea pig Alexa488 (A11073; RRID:AB_10562573), goat anti-guinea pig Alexa568 (A11075; RRID:AB_10563254), donkey anti-mouse Alexa647 (A31571; RRID:AB_10584497). The sections were washed in H_2O, dried and mounted in DAKO fluorescence mounting medium (Dako, Baar, Switzerland). Imaging was performed on a Leica SP2 (Figs. 1, S1, S3A) or Zeiss LSM 700 confocal microscopes using 40x oil immersion objectives. For quantification of Syt1 expression level (Figs. 5C, S4), ROIs were hand-drawn around individual calyceal profiles in VGluT2 channel, after which the binary masks were generated by thresholding the VGluT2 fluorescence within these ROIs. Syt1 fluorescent signal intensity was sampled using the obtained masks from the Syt1 channel, and the local background measured from a ROI outside the calyx area (inside the postsynaptic cell) was subtracted using a custom macro in IgorPro.

For the western blot analysis of Syt9 expression (Fig. 3B; done in adult female $Syt9^{+/+}$ and $Syt9^{-/-}$ mice), a total amount of 0.3 mg brain tissue homogenates boiled in SDS were run per lane on two 10% polyacrylamide gels (mini-protean III system, Bio-Rad Laboratories, Hercules, CA), and the gels were transferred onto identical PVDF membranes (Bio-Rad). Due to close apparent band sizes of Syt9 and β-actin, the two membranes were blotted separately using rabbit anti-Syt5/9 (1:1000; see above) and mouse anti β-actin (1:2500; BioVision 3598-100, San Francisco, CA; RRID:AB_2242350) primary antibodies overnight at 4°C in 1:3 Odyssey Blocking buffer (LI-COR, Lincoln, NE). The secondary antibodies were IRDye 800 conjugated donkey anti-rabbit (Rockland Immunochemicals, Limerick, PA; cat. 611-732-127; RRID:AB_220158) and donkey anti-mouse (LI-COR cat. 926-32212; RRID:AB_621847), respectively, incubated at 1:5000 dilution in 1:2 blocking buffer for 40 min at RT, and imaged on a LI-COR Odyssey scanner. As a positive control, the lysate of E2T adenovirus packaging cells was used, harvested 72 h post-infection with the Hsyn1-MycSyt9::Hsyn1-eGFP adenovirus (the same as used in the Syt9 rescue experiments; Fig. 7).

Supplemental Experimental Procedures for transmission electron microscopy and serial-section 3D reconstruction of the active zones

Preparation of samples containing MNTB principal cells, transmission EM imaging of calyceal presynaptic terminals and three-dimensional reconstruction of single active zones was done as previously described (Knott et al., 2002; Han et al., 2011). Briefly, mice at the age of P14 were anesthetised with pentobarbital and transcardially perfused with PBS, followed by 2% paraformaldehyde / 2.5% glutaraldehyde fixative mix in 0.1 M phosphate buffer (pH 7.4). Transverse 70 µm thick brainstem sections containing MNTB were cut with a vibratome (Leica VT1200), washed in 0.1 M cacodylate buffer (pH 7.4) and post-fixed in 1% osmium tetroxide and 1.5% potassium ferrocyanide, followed by staining in 1% uranyl acetate. After dehydration in 50-70-90-95-100% graded alcohol series, the sections were sequentially embedded in propylene oxide, 1:1 mix of propylene oxide and Durcupan epoxy resin (Sigma), and finally in pure resin, followed by polymerization between two cover glasses at 60˚C overnight. The tissue block was trimmed such that the central part of MNTB remained, and then sectioned at 50 nm thickness and collected onto formvar support films on single-slot grids. After staining with 1.0 % lead citrate, the serial sections were imaged in a Philips CM10 transmission electron microscope operated at 80 kV using 12500-19000x magnification settings. 3D-reconstructions of each individual AZ from the series of EM images was then performed using TrackEM2 application for FIJI (Cardona et al., 2010). Images were aligned by translation and rotation to form a stack covering the single AZs, and the profiles of presynaptic membrane, presynaptic density and vesicles (each vesicle represented by a sphere) were manually outlined in TrackEM2 in order to render a three-dimensional model of the AZ membrane and the adjacent pool of vesicles. From these models, the active zone areas and the closest membrane-to-membrane distances between each vesicle and active zone surface (presynaptic density) were calculated (Fig. S2).

Supplemental References

Cardona, A., Saalfeld, S., Preibisch, S., Schmid, B., Cheng, A., Pulokas, J., Tomancak, P., and Hartenstein, V. (2010). An integrated micro- and macroarchitectural analysis of the Drosophila brain by computer-assisted serial section electron microscopy. PLoS Biol. *8*.

Chatonnet, F., Wrobel, L.J., Mezieres, V., Pasqualetti, M., Ducret, S., Taillebourg, E., Charnay, P., Rijli, F.M., and Champagnat, J. (2007). Distinct roles of Hoxa2 and Krox20 in the development of rhythmic neural networks controlling inspiratory depth, respiratory frequency, and jaw opening. Neural. Dev. *2*, 19.

Clements, J.D., and Bekkers, J.M. (1997). Detection of spontaneous synaptic events with an optimally scaled template. Biophys. J. *73*, 220-229.

Knott, G.W., Quairiaux, C., Genoud, C., and Welker, E. (2002). Formation of dendritic spines with GABAergic synapses induced by whisker stimulation in adult mice. Neuron *34*, 265-273.

Kochubey, O., and Schneggenburger, R. (2015). Ca^{2+} Uncaging in Nerve Terminals: A Three-Point Calibration Procedure. Cold Spring Harbor protocols *2015*, 761-768.

Meyer, A.C., Neher, E., and Schneggenburger, R. (2001). Estimation of quantal size and number of functional active zones at the calyx of Held synapse by nonstationary EPSC variance analysis. J. Neurosci. *21*, 7889-7900.

Zhou, H., and Beaudet, A.L. (2000). A new vector system with inducible E2a cell line for production of higher titer and safer adenoviral vectors. Virology *275*, 348-357.